

# Epitaxy of hexagonal $\text{ABO}_3$ quantum materials


Cite as: Appl. Phys. Rev. **9**, 031309 (2022); <https://doi.org/10.1063/5.0098277>

Submitted: 06 May 2022 • Accepted: 09 August 2022 • Published Online: 21 September 2022

 Johanna Nordlander,  Margaret A. Anderson,  Charles M. Brooks, et al.

## COLLECTIONS

Paper published as part of the special topic on [Quantum Materials and 2D superlattices](#)

 This paper was selected as Featured



View Online



Export Citation



CrossMark

## ARTICLES YOU MAY BE INTERESTED IN

[Flexible organic transistors for neural activity recording](#)

Applied Physics Reviews **9**, 031308 (2022); <https://doi.org/10.1063/5.0102401>

[Two-dimensional material templates for van der Waals epitaxy, remote epitaxy, and intercalation growth](#)

Applied Physics Reviews **9**, 031305 (2022); <https://doi.org/10.1063/5.0090373>

[Spin manipulation by giant valley-Zeeman spin-orbit field in atom-thick  \$\text{WSe}\_2\$](#)

Applied Physics Reviews **9**, 031402 (2022); <https://doi.org/10.1063/5.0089162>

Applied  
Physics Letters

SPECIAL TOPICS

Submit Today!

# Epitaxy of hexagonal $ABO_3$ quantum materials

Cite as: Appl. Phys. Rev. **9**, 031309 (2022); doi: [10.1063/5.0098277](https://doi.org/10.1063/5.0098277)

Submitted: 6 May 2022 · Accepted: 9 August 2022 ·

Published Online: 21 September 2022



View Online



Export Citation



CrossMark

Johanna Nordlander,<sup>1</sup>  Margaret A. Anderson,<sup>1</sup>  Charles M. Brooks,<sup>1</sup>  Megan E. Holtz,<sup>2</sup> and Julia A. Mundy<sup>1,a)</sup> 

## AFFILIATIONS

<sup>1</sup>Department of Physics, Harvard University, Cambridge, Massachusetts 02138, USA

<sup>2</sup>Department of Metallurgy and Materials Engineering, Colorado School of Mines, Golden, Colorado 80401, USA

**Note:** This paper is part of the special collection on Quantum Materials and 2D superlattices

<sup>a)</sup>Author to whom correspondence should be addressed: [mundy@fas.harvard.edu](mailto:mundy@fas.harvard.edu)

## ABSTRACT

Hexagonal  $ABO_3$  oxides ( $A, B = \text{cation}$ ) are a class of rich materials for realizing novel quantum phenomena. Their hexagonal symmetry, oxygen trigonal bipyramid coordination, and quasi-two dimensional layering give rise to properties distinct from those of the cubic  $ABO_3$  perovskites. As bulk materials, most of the focus in this class of materials has been on the rare-earth manganites,  $RMnO_3$  ( $R = \text{rare earth}$ ); these materials display coupled ferroelectricity and antiferromagnetic order. In this review, we focus on the thin-film manifestations of the hexagonal  $ABO_3$  oxides. We cover the stability of the hexagonal oxides and substrates which can be used to template the hexagonal structure. We show how the thin-film geometry not only allows for further tuning of the bulk-stable manganites but also allows for the realization of metastable hexagonal oxides such as the  $RFeO_3$  that combine ferroelectricity with weak ferromagnetic order. The thin-film geometry is a promising platform to stabilize additional metastable hexagonal oxides to search for predicted high-temperature superconductivity and topological phases in this class of materials.

Published under an exclusive license by AIP Publishing. <https://doi.org/10.1063/5.0098277>

## TABLE OF CONTENTS

I. INTRODUCTION .....	1
II. STABILITY OF THE HEXAGONAL $ABO_3$ PHASE....	3
III. SUBSTRATE TEMPLATES FOR HEXAGONAL $ABO_3$ THIN FILMS.....	4
IV. EPITAXY OF BULK-STABLE HEXAGONAL $ABO_3$ COMPOUNDS.....	5
V. EPITAXY OF METASTABLE HEXAGONAL $ABO_3$ COMPOUNDS.....	9
VI. OUTLOOK .....	12

## I. INTRODUCTION

Complex oxides display some of the most exotic physical states known. The subtle interplay of Coulomb interactions, electron–lattice coupling, and spin/orbital ordering gives rise to phenomena as diverse as high-temperature superconductivity and ferromagnetism. Synthesizing complex oxides in the thin-film form offers further opportunities to tune the ground state. Here, strain imparted from a substrate, dimensionality in a superlattice architecture, or charge transfer/coupling at an interface can unleash further emergent properties not present in the parent compounds.<sup>1,2</sup> Moreover, complex oxide thin films not only offer opportunities to study diverse physical

phenomena but also could be harnessed for a number of next-generation applications.<sup>3</sup>

To date, however, much of the work on complex oxides in the thin-film form has focused on cubic perovskite oxides. This review focuses on a different class of oxides with the same  $ABO_3$  stoichiometry ( $A, B = \text{cations}$ ), the hexagonal oxides. As shown in Fig. 1(a), the crystal structure differs from that of the cubic perovskites: the  $B$ -site cation is surrounded by a trigonal bipyramid arrangement of oxygen atoms in contrast to the oxygen octahedra characteristic of the perovskite oxides. Planes of corner-sharing trigonal bipyramids are layered with planes of the  $A$ -site cation in a quasi-two-dimensional structure. (We refer the reader to an excellent recent review<sup>4</sup> that covers a more generic class of hexagonal oxides that include face-sharing polyhedra and other structural types.) We focus on this class of materials not to generically expand the study of oxide compounds but specifically because the distinct symmetry and the crystal field environment can offer unique opportunities to realize novel properties not present in the cubic perovskite oxides.

While considerably less studied than the perovskite oxides, the hexagonal  $ABO_3$  materials also display a rich array of physical phenomena (see overview in Table 1). The most commonly studied hexagonal oxides are the rare-earth manganites,  $RMnO_3$ , where  $R = \text{Sc, Y, In, and Dy-Lu}$ . These materials display robust improper

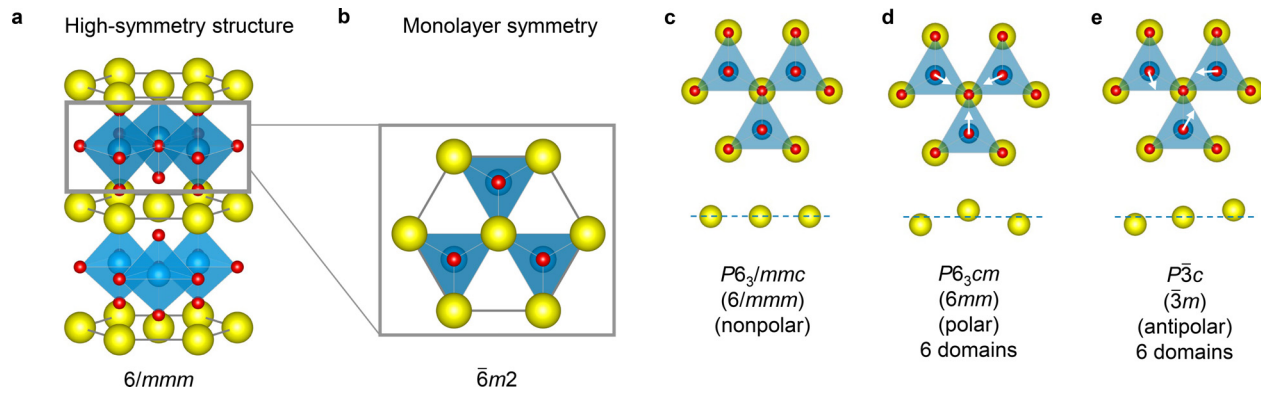


**FIG. 1.** Crystal structure and symmetry of the hexagonal  $ABO_3$  compounds. The A-site, B-site, and oxygen atoms are shown in yellow, blue, and red, respectively. (a) The parent centrosymmetric  $P6_3/mmc$  structure that is nonpolar with point symmetry  $6/mmm$ . (b) A slice of the half-unit-cell plane as indicated in the box in (a), projected down the [001] crystallographic zone axis. The B-site cations sit on a trigonal lattice with a locally lowered (noncentrosymmetric) symmetry compared to the full unit-cell structure, which consists of two of these B-site planes rotated  $60^\circ$  with respect to each other, sandwiched between the triangular rare-earth layers. (c)–(e) Displacement patterns found in hexagonal  $ABO_3$  compounds and the corresponding unit-cell space (point) symmetry groups. (c) The nonpolar parent structure, for reference. (d) The polar phase has a coordinated tilting of three  $BO_5$  trigonal bipyramids toward a trimerization center accompanied by a “down-up-down” displacement pattern of A site ions along the c axis. (e) The antipolar phase consists of intermediate tilt angles  $30^\circ$  away from the polar structure and a “down-middle-up” displacement pattern on the A site along the c axis.

ferroelectricity well above room temperature<sup>5,6</sup> as a consequence of a lattice trimerization involving a coordinated tilting of the  $MnO_5$  bipyramids and a distortion of the rare-earth ion layers<sup>7,8</sup> (see Fig. 1). Notably, at low temperature, this ferroelectricity coexists and is coupled with antiferromagnetic order,<sup>9–13</sup> as shown in Fig. 2. More recently, the hexagonal  $RFeO_3$  compounds have been studied:<sup>14–16</sup> in these compounds, there is a proposed coupling of ferroelectricity with weak ferromagnetic order.<sup>17</sup> In addition to the proposed uses in energy-efficient magnetoelectric spin-orbit logic devices,<sup>18</sup> the ferroelectricity and ferroelectric domain walls in the hexagonal manganites and ferrites have emerged as fascinating model systems to study

diverse physical phenomena. The ferroelectric domain walls display tunable metallic conductivity.<sup>19–21</sup> The emergence of the ferroelectric domain structure, exhibiting a topologically protected vortex pattern, is further a platform to explore the Kibble–Zurek framework and spontaneous symmetry breaking in a condensed matter system.<sup>22–24</sup> The structural phase transitions have also been proposed to display Higgs and Goldstone physics.<sup>25</sup>

In addition to multiferroics, the hexagonal  $ABO_3$  family offers additional prospects to stabilize emergent magnetic ground states including the elusive quantum spin liquid state. In a quantum spin liquid, spins are highly correlated and strongly frustrated due to the crystal symmetry (e.g., triangular, honeycomb, or Kagome). The resulting degeneracy between competing ground state spin configurations leads to a highly entangled state that resists macroscopic magnetic ordering to the lowest temperatures.<sup>26</sup> Importantly, the “spinon” quasiparticle excitations of this system can be itinerant Majorana fermions with a gapless dispersion of relevance to quantum computing.<sup>27</sup> In addition to the intrinsic triangular symmetry of the hexagonal  $ABO_3$  oxides, chemical doping or lattice distortions can construct a honeycomb or Kagome lattice with additional opportunities to realize frustrated magnetism. For example,  $InCu_{2/3}V_{1/3}O_3$  has both  $Cu^{2+}$  and  $V^{5+}$  on the B-site lattice. These cations in the 2:1 ratio arrange such that the  $Cu^{2+}$  forms a honeycomb lattice,<sup>28,29</sup> as shown in Fig. 3(b). Here, the honeycomb  $Cu^{2+}$  atoms seem to order antiferromagnetically<sup>30</sup> rather than behave as a quantum spin liquid. (This system could also be proximate to chiral superconductivity.<sup>31</sup>) In the  $LaCu_{3/4}Mo_{1/4}O_3$  compound, the 3:1 ratio of  $Cu^{2+}$  to  $Mo^{6+}$  generates a Kagome arrangement of copper atoms<sup>32</sup> depicted in Fig. 3(c). Finally, we note that the “up-up-down” ferroelectric trimerization on the A-site generates a honeycomb arrangement as well,<sup>33</sup> as shown in Fig. 3(d). In  $TbInO_3$ , the resulting magnetic frustration on the terbium sublattice leads to a lack of order to the lowest temperatures and  $TbInO_3$  is a promising quantum spin liquid candidate.<sup>33</sup>

Finally, the hexagonal oxides have distinct oxygen sublattices to their perovskite counterparts. In contrast to the oxygen octahedra

**TABLE I.** Observed and predicted properties of the  $ABO_3$  hexagonal materials.

Compound	Properties	References
$RMnO_3$ , $R = Sc, Y, Dy-Lu$	Multiferroic	12
$RMnO_3$ , $R = Sc, Y, Dy-Lu$	Photovoltaic	37 and 38
$YIn_{1-x}Mn_xO_3$	Blue pigment	39
$DyMnO_3$	Ion/electron conductor	35
$RMnO_3$	Oxygen storage	35 and 40
$RFeO_3$ , $R = Lu, Yb, Sc$	Multiferroic	14–16
$DyFeO_3$	Antiferroelectric	41
$YFeO_3, InFeO_3$	Photocatalyst/ water splitting	42–44
$R_2CuTiO_6$ , $R = Y,$ $Dy, Ho, Er, \text{ and } Yb$	High- $\kappa$ dielectric	45
$TbInO_3$	Quantum spin liquid candidate	33 and 46
$YCrO_3, YVO_3$	Predicted topological semi-metal	47
$YNiO_3$	Predicted superconductor	36 and 48

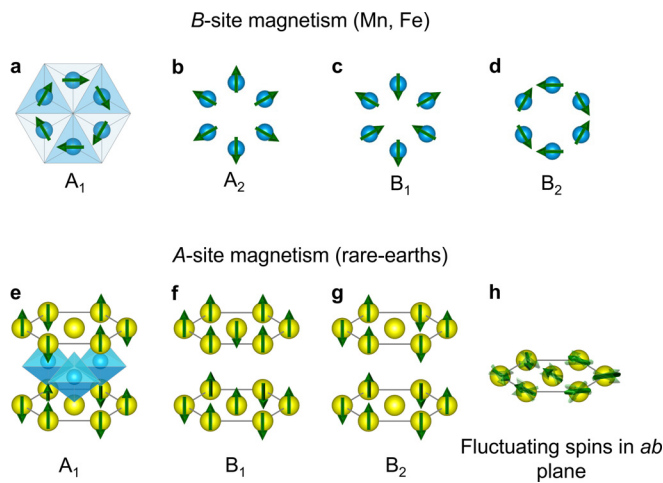


**FIG. 2.** Magnetic order in the hexagonal  $ABO_3$  compounds. (a)–(d) Spin orientation on the  $B$ -site. (e)–(h) Spin orientation on the  $A$ -site, for  $A$  = rare-earth element. The fully ferromagnetically ordered  $A_2$  configuration is not shown. (h) In the absence of  $B$ -site magnetism, the geometric frustration experienced by the rare-earth moments on the triangular lattice can lead to suppressed ordering temperatures or spin fluctuations persistent to the lowest temperatures.

characteristic of the perovskites, the trigonal bipyramid intrinsic to the hexagonal  $ABO_3$  structure has two distinct oxygen atoms located at the apical and in-plane position. These oxygen atoms can have different bonding to the transition metal atom,<sup>34</sup> which, in principle, can be harnessed for oxygen ion conductivity.<sup>35</sup> There have also been

theoretical predictions that the crystal field splitting surrounding the transition metal oxide could be harnessed to stabilize superconductivity in hexagonal nickelates (mimicking the electronic structure of the superconducting cuprates and pnictides).<sup>36</sup>

Thin-film manifestations of these hexagonal oxides offer further opportunities to not only scale down the materials to fundamental thickness limits<sup>49</sup> and heterostructure them to realize additional functional properties<sup>50</sup> but furthermore to exploit epitaxy and layering<sup>51</sup> to stabilize metastable compounds. Thin-film epitaxy of the hexagonal  $ABO_3$  oxides offers additional challenges in comparison to the cubic perovskite oxides. In this review, we first summarize the stability of the hexagonal  $ABO_3$  compounds. We then describe the thin-film deposition of the bulk-stable  $RMnO_3$  compounds, including the lattice matching of the hexagonal crystal structure to commercially available substrates. We finally discuss the use of epitaxy to expand the stability of this phase.

## II. STABILITY OF THE HEXAGONAL $ABO_3$ PHASE

Compounds with the  $ABO_3$  stoichiometry can form a variety of cubic, orthorhombic, and hexagonal phases. The formation of the hexagonal phase is dictated by both structural stability and the electronic energy of the  $B$ -site in the trigonal bipyramid oxygen coordination complex. The structural stability of the competing cubic perovskite phase can be estimated with the tolerance factor ( $t$ ), a geometric quantity based on the ionic radii ( $r$ ) of constituent atoms that indicates how well a given  $ABO_3$  compound fits in the cubic perovskite structure. Here,  $t$  is given by

$$t = \frac{(1/\sqrt{2}) \text{face diagonal}}{\text{unit-cell length}} = \frac{r_A + r_O}{\sqrt{2}(r_B + r_O)}.$$

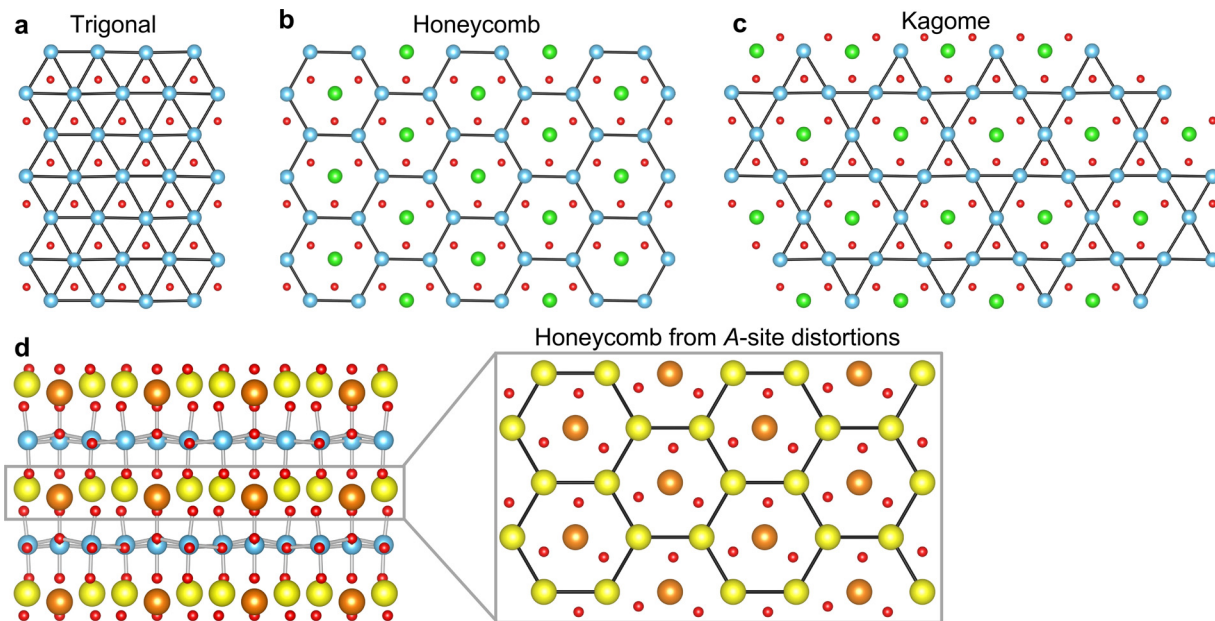


**FIG. 3.** Symmetry embedded in the  $ABO_3$  structure. (a) A slice of the  $B$ -site plane from the  $ABO_3$  structure, projected down the  $[001]$  crystallographic zone axis. The  $B$ -site cations follow a trigonal pattern. (b) and (c) Replacement of the  $B$ -site cation with a different element at  $1/4$  or  $1/3$  filling can construct a honeycomb or Kagome lattice, respectively. (d) The honeycomb lattice is also formed on the  $A$  site of the  $P6_3cm$  structure where the yellow atoms are displaced up and the orange atoms displaced down in the “up–up–down” polarization direction. Oxygen is shown in red,  $A$ -site cations are shown in yellow/orange, and  $B$ -site cations are shown in blue/green.

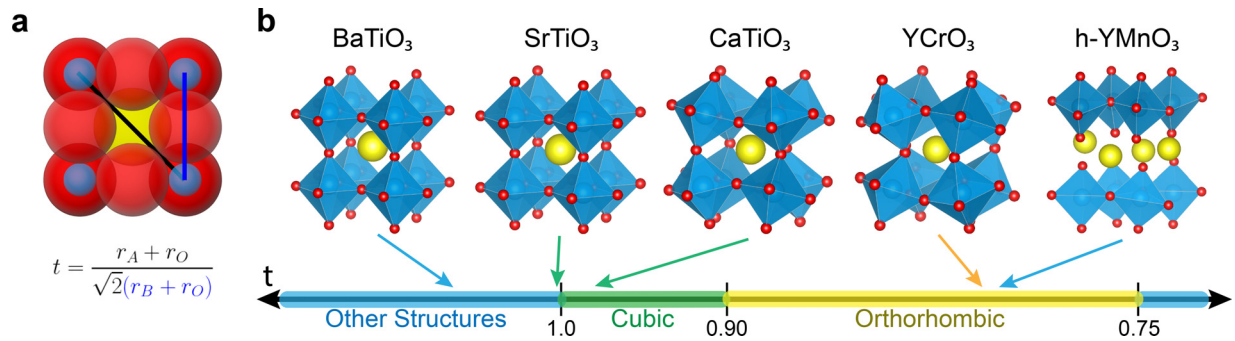


**FIG. 4.** The perovskite Goldschmidt tolerance factor. (a) The tolerance factor,  $t$ , is calculated as the ratio of  $\frac{1}{\sqrt{2}}$  times a face diagonal ( $2r_A + 2r_O$ ) and a unit cell length ( $2r_B + 2r_O$ ).  $t = 1$  for ions which perfectly pack into the cubic perovskite structure. (b) Examples of  $ABO_3$  compounds with various tolerance factors and the approximate regions of stability for each structure. As  $t$  decreases from 1, the  $B$ -site octahedral cages tilt and bond lengths change, forming successively lower-symmetry structures. The cubic perovskite phase with space group  $Pm\bar{3}m$  occurs for approximately  $0.90 < t < 1.0$ , while the orthorhombic phase with space group  $Pnma$  or  $Pbnm$  occurs for  $0.75 < t < 0.90$ .<sup>53</sup> Outside of this range, other structures including a hexagonal phase with space group  $P6_3cm$ , a tetrahedral phase, and the hexagonal ilmenite structure are formed. The tolerance factors for  $BaTiO_3$ ,  $SrTiO_3$ ,  $CaTiO_3$ ,  $YCrO_3$ , and  $YMnO_3$  are 1.07, 1.01, 0.97, 0.83, and 0.81, respectively.

The tolerance factor is 1 for  $A$  and  $B$  ions which can be packed into a perfect cubic perovskite. The well-known perovskite  $SrTiO_3$  has  $t = 1.01$ , when calculated with  $r_A = r_{Sr^{2+}(XII)} = 144$  pm,  $r_B = r_{Ti^{4+}(VI)} = 60.5$  pm, and  $r_O = r_{O^{2-}(II)} = 135$  pm, where  $r_{Sr^{2+}(XII)}$  is the ionic radius of  $Sr^{2+}$  with 12-fold oxygen coordination.<sup>52</sup> As  $t$  deviates from 1, the structure is distorted from a cubic perovskite (Fig. 4). For example,  $YCrO_3$  with  $t = 0.83$  forms a distorted orthorhombic perovskite phase. A tolerance factor far from 1 does not imply the stability of the hexagonal phase but instead identifies candidate compounds that are less stable in the cubic perovskite phase.  $YMnO_3$  and  $YFeO_3$ , both with  $t = 0.81$ , have less structural stability in the cubic perovskite phase. Despite having the same tolerance factor,  $YFeO_3$  assumes an orthorhombic perovskite structure whereas  $YMnO_3$  crystallizes in a hexagonal phase.

In addition to the structural stability of competing phases, electronic stability impacts the bulk-stable crystal structure. The electronic stability of the hexagonal oxides is based on the crystal field splitting of the  $d$ -orbitals of the  $B$ -site transition metal ions with trigonal bipyramid (fivefold) oxygen coordination. With this ligand geometry, the five  $d$ -orbitals split into three energy levels: two doubly degenerate lower energy levels and one non-degenerate high energy level (Fig. 5). In contrast, a perovskite with octahedral (sixfold) coordination on the  $B$ -site has two energy levels: the three-fold degenerate  $t_{2g}$  low energy level and the doubly degenerate  $e_g$  high energy level.  $Fe^{3+}$ , with the electron configuration  $[Ar]3d^5$ , is more stable in the octahedral coordination, which avoids occupying the highest energy level in the trigonal bipyramid configuration. As a result,  $RFeO_3$  compounds are more stable as orthorhombic perovskites. In contrast,  $Mn^{3+}$ , with configuration  $[Ar]3d^4$ , is more stable in a trigonal bipyramid complex where the four valence electrons populate the four lower energy orbitals. With octahedral coordination,  $Mn^{3+}$  forms a degenerate high-spin state with its fourth valence electron in either of the two  $e_g$  orbitals; these perovskite manganites are Jahn–Teller active.<sup>54</sup> The electron in the higher energy orbitals lowers the stability of the compound. Thus, the  $RMnO_3$  compounds form a hexagonal crystal structure for small  $R$  ( $R = Sc, Y, Dy-Lu$ ), as shown in Fig. 6.

In Fig. 7, we summarize the elements which have been found in the hexagonal  $ABO_3$  polymorph. In contrast to the cubic perovskites

where almost every element on the periodic table can occupy one of the three lattice sites,<sup>2,56</sup> the hexagonal structure can form with more limited chemical compositions. Only six cations are known to fully occupy the  $B$ -site although there is a much wider range of elements which can be stabilized as dopants or as partial occupants of this lattice site. We note that thin-film stabilization is a powerful platform for synthesizing phases which are metastable as bulk crystals.<sup>57</sup> While  $YMn_{1-x}Fe_xO_3$  could be stabilized in the  $P6_3cm$  structure for  $x < 0.3$  in bulk crystals, epitaxial stabilization has led to the construction of  $LuFeO_3$  with the hexagonal  $P6_3cm$  structure.<sup>14–16,58</sup> Explicit stromataxy—precise control over the layering—has enabled further stability of this phase.<sup>51</sup>

### III. SUBSTRATE TEMPLATES FOR HEXAGONAL $ABO_3$ THIN FILMS

While sputtering, metal–organic chemical vapor deposition (MOCVD), molecular-beam epitaxy (MBE), and pulsed laser deposition (PLD) have emerged as powerful tools to synthesize oxide materials in thin-film form, there are unique challenges to the deposition of hexagonal oxides. In contrast to the more commonly studied perovskite oxides, where there is a “menu” of isostructural, commercially available perovskite substrates<sup>59</sup> with

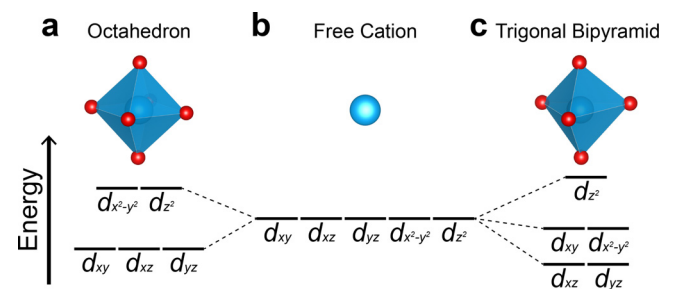


**FIG. 5.** The  $d$ -orbital energy configuration for ions with (a) octahedral oxygen coordination (as for  $B$ -site cations in cubic perovskites), (b) free ions, and (c) trigonal bipyramid coordination (as for  $B$ -site cations in hexagonal  $ABO_3$  materials).

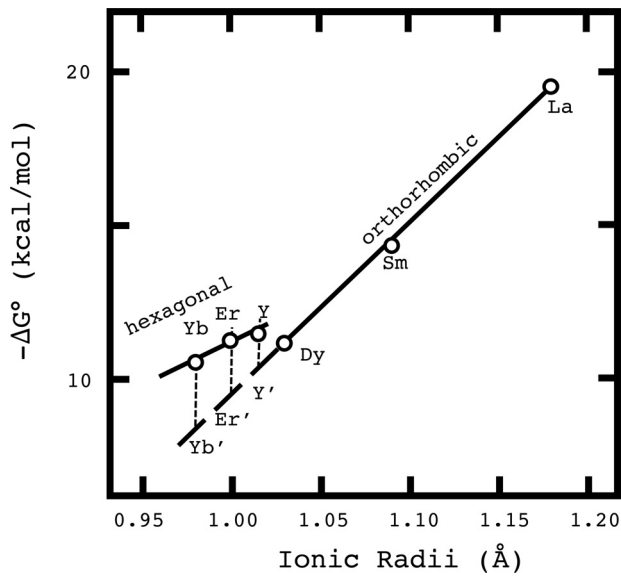


**FIG. 6.** The dependence of free energy of formation on rare-earth ionic radii,  $RE^{3+}$  in  $RMnO_3$ , at  $1200^\circ$ .  $RE'$  indicates the estimated free energy of formation for the perovskite structure in high pressure. Reprinted with permission from Kamata *et al.*, *Mater. Res. Bull.* **14**, 1007–1012 (1979). Copyright 1979 Elsevier.<sup>55</sup>

various lattice constants, the most readily available oxide substrate used to stabilize hexagonal films is  $Al_2O_3$ . This substrate is not well lattice-matched to all desired hexagonal  $ABO_3$  films. In addition to hexagonal oxides, cubic substrates can be used in the (111) orientation. [Figure 8](#) shows the lattice mismatch between the prototypical

hexagonal  $YMnO_3$  and (0001)-oriented  $Al_2O_3$ , (111)-oriented cubic oxides  $MgO$ ,  $MgAl_2O_4$ ,  $(ZrO_2)_{0.905}(Y_2O_3)_{0.095}$  (9.5 mol. % yttria-stabilized zirconia, YSZ), and (111)-oriented metallic platinum. In addition to directly aligning on the substrate,  $YMnO_3$  could also adopt a  $30^\circ$  rotation with respect to the substrate orientation [this would be analogous to the  $45^\circ$  rotation cubic perovskites might assume in the (001) direction]. [Figure 9](#) summarizes the lattice matching between  $P6_3cm$   $YMnO_3$  and many commercially available substrates. While (111)-oriented cubic perovskites also have the correct symmetry, our experience is that these substrates seed the (111)-perovskite film rather than the intended hexagonal polymorph.

#### IV. EPITAXY OF BULK-STABLE HEXAGONAL $ABO_3$ COMPOUNDS

Epitaxial thin-film synthesis of hexagonal  $ABO_3$  materials was first achieved for the prototypical family of hexagonal rare-earth manganites ( $RMnO_3$ ). In particular, initial focus centered on the epitaxy of  $YMnO_3$ , which remains the most intensely studied member of the hexagonal  $ABO_3$  materials. The first epitaxial synthesis of hexagonal  $YMnO_3$  in 1996 was motivated by the material’s high-temperature uniaxial ferroelectricity combined with its suitability for integration with silicon as nonvolatile ferroelectric memories.<sup>60</sup> Following the demonstration of magnetoelectric coupling effects in hexagonal  $RMnO_3$  bulk crystals,<sup>11,12</sup> interest shifted toward thin-film manifestations of such multiferroic properties and potential magnetoelectric effects. In 2006, Laukhin *et al.* demonstrated electrical control of magnetism in a Permalloy/ $YMnO_3$  thin-film heterostructure<sup>61</sup> [see [Fig. 10\(a\)](#)]. A giant flexoelectric effect was further observed in strained  $HoMnO_3$  films,<sup>62</sup> which could be used to tune the ferroelectric properties [[Fig. 10\(b\)](#)]. The discovery of the topologically protected vortex

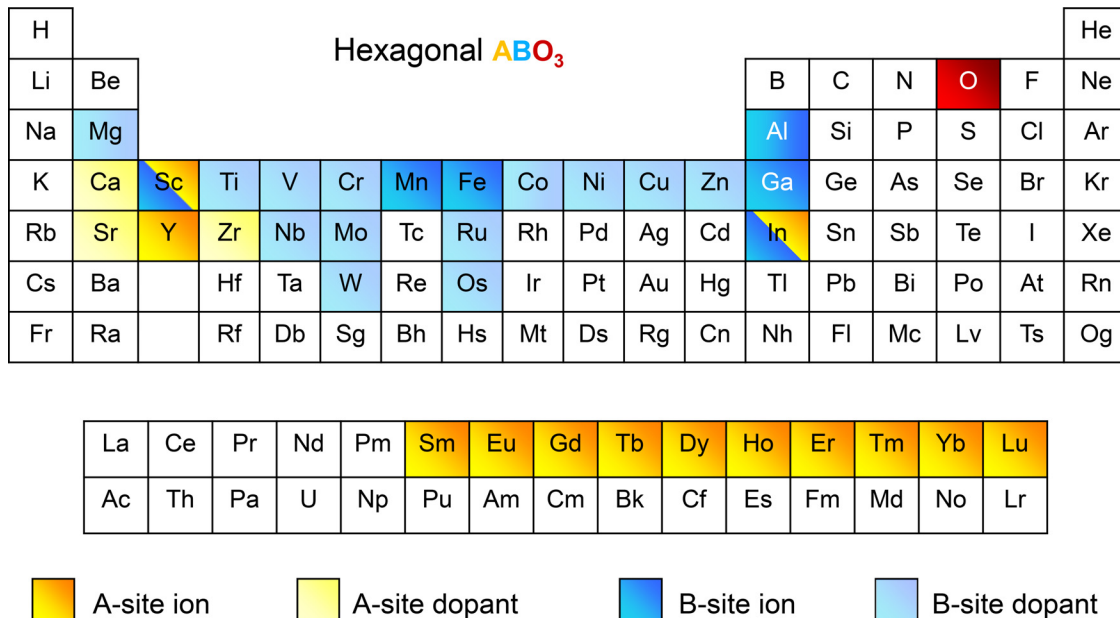


**FIG. 7.** Periodic table indicating the elements that can be stabilized in the hexagonal  $ABO_3$  phase. A-site ions are colored in yellow and B-site ions are colored in blue. We color in light yellow/blue the elements which can be found to partially occupy the site.

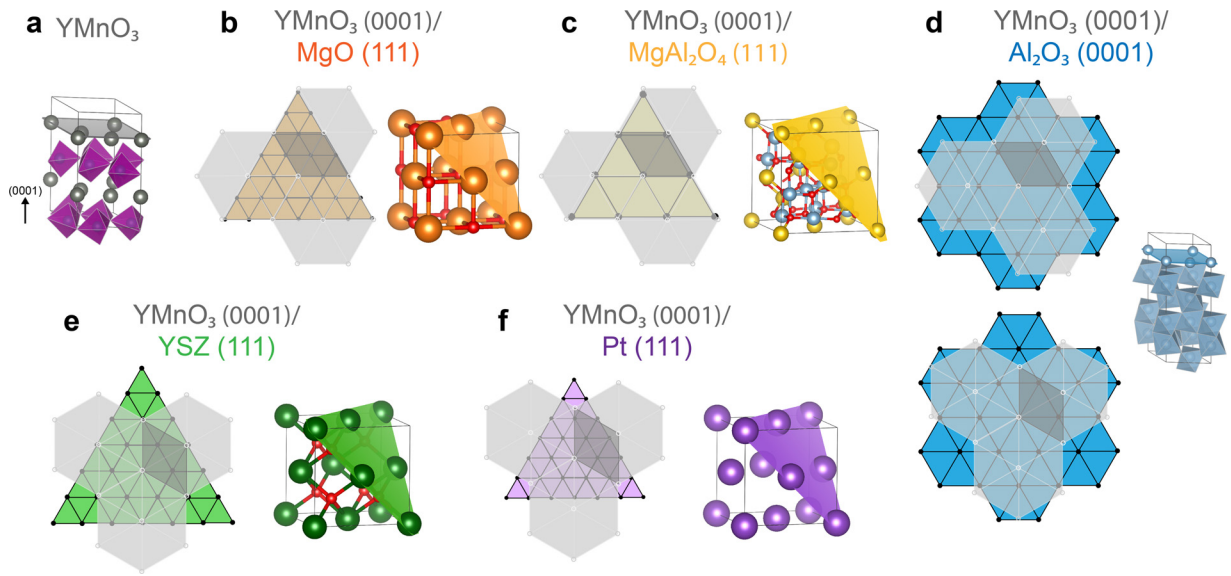


**FIG. 8.** Lattice matching between  $\text{YMnO}_3$  and common substrates. (a) The structure of  $\text{YMnO}_3$  with a (0001) plane of yttrium atoms highlighted in gray. (b) Lattice matching between yttrium atoms in the (0001) plane of  $\text{YMnO}_3$  in gray and the magnesium atoms in the (111) plane of  $\text{MgO}$  in orange. Lattice mismatch (with a factor of 2):  $-2.9\%$ . (c) Lattice mismatch between  $\text{YMnO}_3$  in gray and the magnesium atoms of  $\text{MgAl}_2\text{O}_4(111)$  in yellow. Lattice mismatch:  $-7.0\%$ . (d) Lattice mismatch of  $\text{YMnO}_3$  with the blue aluminum atoms of  $\text{Al}_2\text{O}_3(0001)$  in two orientations: aligned [lattice mismatch (with a factor of  $\frac{2}{3}$ ):  $3.4\%$ ] and with a  $30^\circ$  rotation [lattice mismatch (with a factor of  $\frac{2}{3}$ ):  $-10.5\%$ ]. (e) Lattice mismatch between  $30^\circ$  rotated  $\text{YMnO}_3$  and the zirconium atoms of yttria-stabilized zirconia (YSZ) in green. Yttrium is omitted from the YSZ crystal structure for clarity. Lattice mismatch:  $2.6\%$ . (f) Lattice mismatch between  $30^\circ$  rotated  $\text{YMnO}_3$  and the platinum atoms of  $\text{Pt}(111)$ . Lattice mismatch (with a factor of  $\frac{2}{3}$ ):  $4.6\%$ .

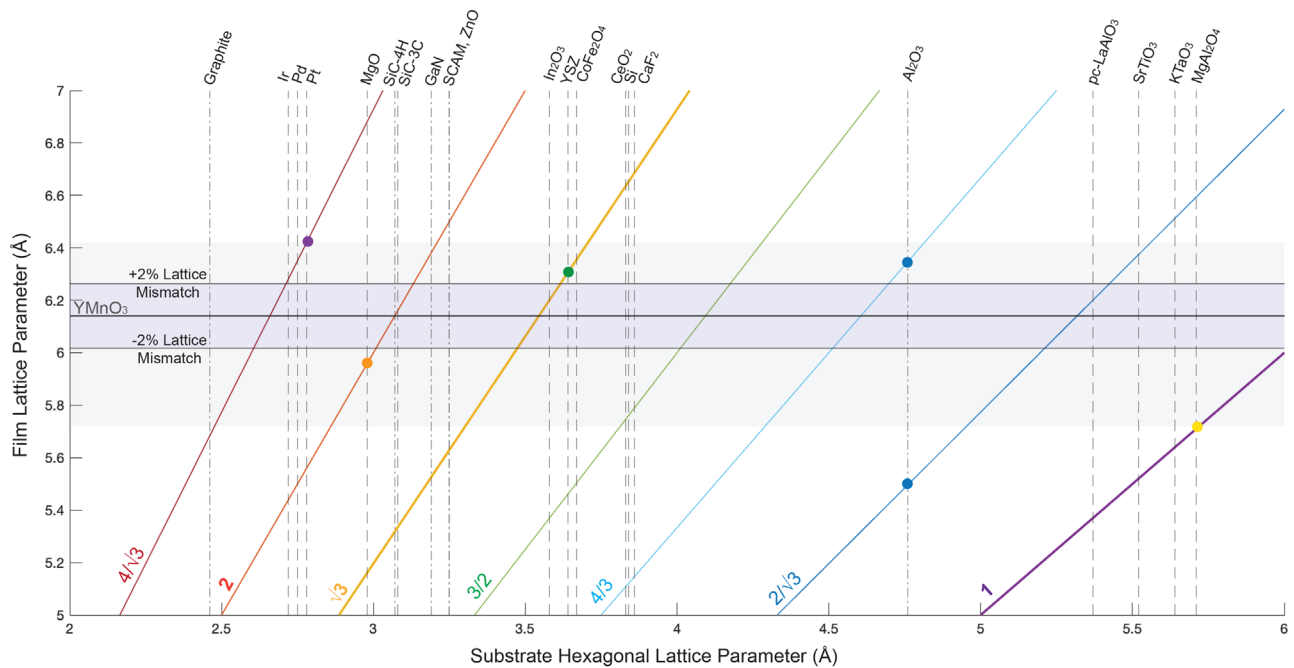


**FIG. 9.** In-plane lattice matching for hexagonal materials. Vertical lines indicate substrate (0001) (dotted-dashed lines) and (111) (dashed lines) in-plane lattice parameters. The intersection between a vertical line and scaling factor indicates a possible effective substrate lattice parameter. The horizontal line at  $6.14 \text{ \AA}$  represents  $\text{YMnO}_3$  and the boundaries for  $\pm 2\%$  lattice mismatch are labeled. The gray region indicates typical hexagonal film lattice parameters. Colored dots correspond to the lattice matching diagrams in **Fig. 8**. The thickness of the scaling factor lines roughly matches their likelihood of being realized, with 1 and  $\sqrt{3}$  the most common.

domain patterns in bulk crystal  $\text{RMnO}_3$  compounds in 2010<sup>19,63</sup> and their related domain-wall functionalities,<sup>20,21</sup> sparked a renewed interest in the multiferroic domain structure and thickness scaling in hexagonal  $\text{RMnO}_3$  thin films. Furthermore, the improper nature of the ferroelectric order in hexagonal  $\text{ABO}_3$  oxides, which is driven by a non-ferroelectric structural distortion, suggests novel avenues for stabilizing and controlling spontaneous ferroelectric polarization in the ultrathin limit.<sup>49,64,65</sup>

To date, the hexagonal phase has been realized as thin films for the entire bulk-stable rare-earth manganite series ( $R = \text{Dy-Lu}$ ,<sup>38,60,66-72</sup>). Epitaxial stabilization additionally extended the series to lighter rare-earth ions down to samarium ( $\text{Sm-Tb}$ ,<sup>67,73-75</sup>) that normally would crystallize in the orthorhombic  $Pnma$  phase as further discussed in Sec. V. Here, hexagonal  $\text{SmMnO}_3$  has been achieved only on an isostructural  $\text{YMnO}_3$  substrate,<sup>73</sup> whereas the other members

can be grown epitaxially on commercially available substrates such as  $\text{YSZ}(111)$ . In addition to the rare-earth series and yttrium, the  $A$ -site of hexagonal manganites can accommodate both scandium and indium. However, to our knowledge, only the (epitaxially stabilized) orthorhombic phase of  $\text{ScMnO}_3$  has been reported in thin films; growth of hexagonal  $\text{InMnO}_3$  remains limited to polycrystalline films reported in the literature.<sup>76</sup> In bulk  $\text{InMnO}_3$ , carefully tuning the defect chemistry or the thermal history of the crystals selects between trimerized domains of either  $P6_3cm$  symmetry [see Fig. 1(d)], just as in the other rare-earth manganites, or anti-polar  $P\bar{3}c1$  symmetry [Fig. 1(e)], as seen at the domain walls between the polar trimerization domains in  $\text{RMnO}_3$ , all the while retaining the vortex domain pattern.<sup>77-79</sup> Epitaxial realization of single-crystalline hexagonal  $\text{InMnO}_3$  thus provides an interesting opportunity for studying the thin-film manifestation of these complementary symmetry properties.

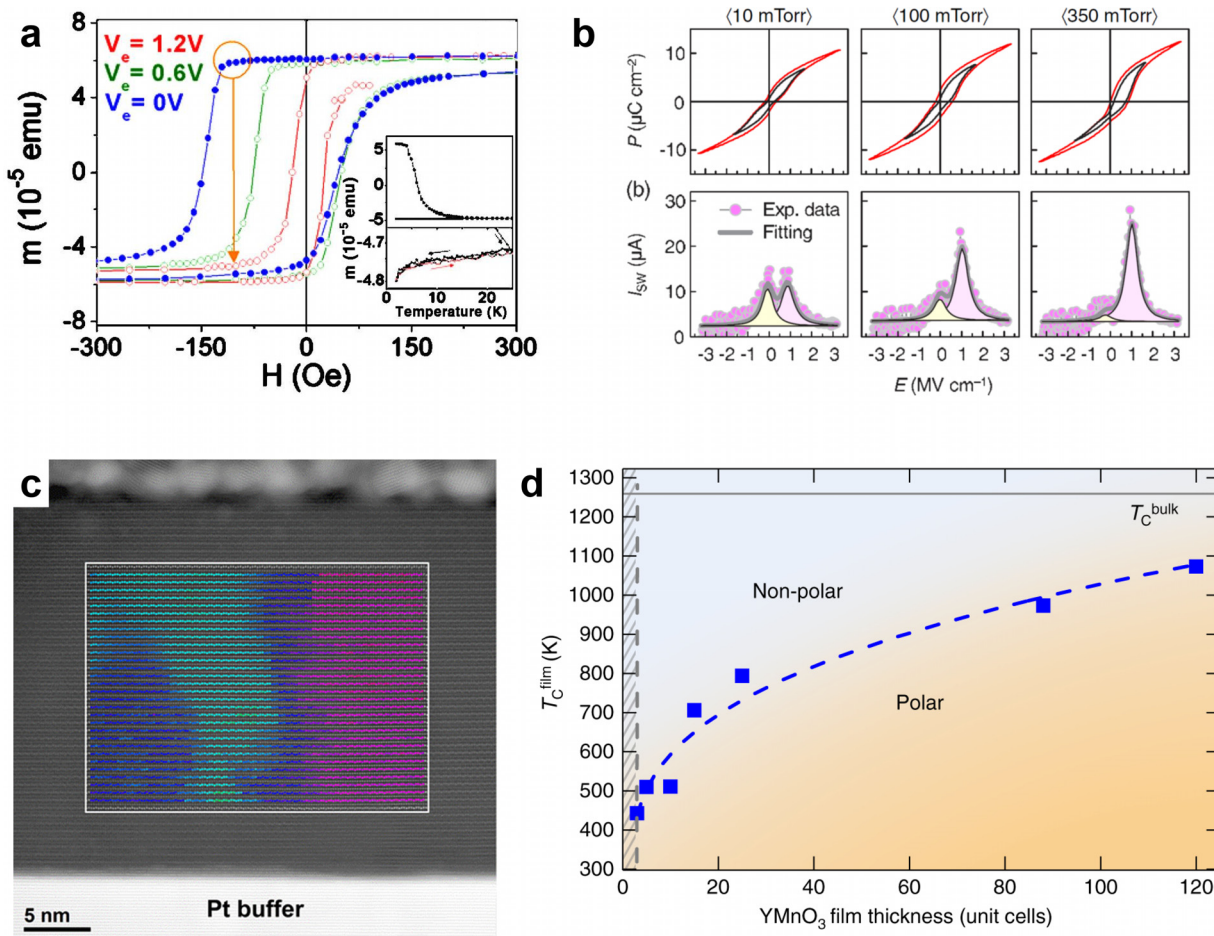


**FIG. 10.** Ferroelectric properties of hexagonal  $\text{RMnO}_3$  thin films. (a) Voltage control of exchange bias in a Permalloy layer through interfacial magnetic exchange in epitaxial multiferroic  $\text{YMnO}_3$  grown on  $\text{Pt}(111)/\text{SrTiO}_3(111)$ . Reprinted with permission from Laukin *et al.*, Phys. Rev. Lett. **97**, 227201 (2006). Copyright 2006 American Physical Society.<sup>51</sup> (b) Modification of ferroelectric hysteresis loops in hexagonal  $\text{HoMnO}_3$  films on  $\text{Pt}(111)/\text{Al}_2\text{O}_3(0001)$  caused by the strain-gradient-induced flexoelectric effect. Reprinted with permission from Lee *et al.*, Phys. Rev. Lett. **107**, 057602 (2011). Copyright 2011 American Physical Society.<sup>62</sup> (c) Improper ferroelectric domain pattern mapped at the atomic scale in hexagonal  $\text{YMnO}_3$  on  $\text{Pt}(111)/\text{YSZ}(111)$  using HAADF-STEM. Each color represents one of six total trimerization domain states, with polarization pointing either up or down. (d) Improper ferroelectric transition temperatures in hexagonal  $\text{YMnO}_3$  films grown on  $\text{YSZ}(111)$  as function of film thickness. (c) and (d) reprinted with permission from Nordlander *et al.*, Nat. Commun. **10**, 5591 (2019). Copyright 2019 Author(s), licensed under a Creative Commons Attribution 4.0 License.<sup>49</sup>



As mentioned in Sec. III, a major challenge in thin-film growth of the hexagonal manganites is the lack of isostructural or lattice-matching substrates. Added to this is a tendency to form crystallographic domains and defects due to close lattice matching between multiple crystallographic orientations of the hexagonal  $\text{RMnO}_3$  structure itself and between  $\text{RMnO}_3$  and the corresponding binary oxide  $\text{R}_2\text{O}_3$ .<sup>80</sup> Indeed, the higher symmetry of cubic substrates such as YSZ compared to that of the layered hexagonal  $\text{ABO}_3$  phase impedes nucleation of a completely single-domain crystalline film and can cause defects such as antiphase boundaries. Thus, careful attention to substrate surface termination may play an important role in reducing the occurrence of these types of defects.<sup>81</sup> The epitaxial quality of  $\text{RMnO}_3$  films is also strongly dependent on substrate temperature during deposition. The hexagonal phase crystallizes down to 690 °C;<sup>82</sup> however, the highest crystalline quality is achieved in the range 750–900 °C. Although hexagonal manganite thin films have been grown on a range of substrates including YSZ(111), Si(111), Pt(111), MgO(111), GaN(0001), ZnO(0001), and *c*-plane  $\text{Al}_2\text{O}_3$ ,<sup>60,61,66,71,83–88</sup> resulting in various degrees of crystallinity, not nearly as many options are commercially available as for their perovskite  $\text{ABO}_3$  counterparts.

Over the past decade, significant improvement of the thin-film crystalline quality of  $\text{RMnO}_3$  has been achieved and epitaxial layer-by-layer thin-film growth with sub-unit-cell thickness precision has recently been demonstrated.<sup>81</sup> Such improvement of structural quality has been crucial to the investigation into the ultrathin manifestation of improper ferroelectric properties and domain structure<sup>49,75,89,90</sup> in this class of materials [Fig. 10(c)]. In particular, the structural distortion transforming the nonpolar  $P6_3/mmc$  phase to the polar  $P6_3cm$  phase and leading to the secondary ferroelectric polarization was shown to be significantly modified by substrate-interface proximity, as demonstrated by a combination of *in situ* high-angle annular dark-field scanning transmission electron microscopy (HAADF-STEM) and optical second harmonic generation (SHG).<sup>49</sup> The resulting threshold thickness for room-temperature polarization in  $\text{YMnO}_3$  on an insulating substrate was determined to be two unit cells [Fig. 10(d)].

In hexagonal  $\text{RMnO}_3$ , the improper ferroelectric order coexists with antiferromagnetic order on the  $\text{Mn}^{3+}$  sublattice below 70–120 K, leading to multiferroicity. Because of the fully compensated nature of this antiferromagnetic order (i.e., lack of net magnetic moment), its thin-film manifestation has been challenging to study.<sup>91</sup> Although neutron diffraction on thicker films of  $\text{YMnO}_3$  (thickness exceeding 400 nm) shows Néel temperatures that closely match the bulk values,<sup>69</sup> similar neutron measurements on thinner films are precluded due to the limited thin-film volume. Moreover, SQUID magnetometry has revealed spin-glass states in oxygen-deficient  $\text{YMnO}_3$  films, indicating the strong influence of oxygen off-stoichiometry on the magnetic order.<sup>70,92</sup> Hence, further work is needed to fully characterize the intrinsic magnetic state of ultrathin hexagonal  $\text{RMnO}_3$ . Additionally, the antiferromagnetic domain size is expected to be significantly reduced in thin films compared with bulk crystals, hampering real-space characterization.<sup>93</sup> Thus, the enigmatic multiferroic coupling of ferroelectric and antiferromagnetic domain patterns observed in  $\text{RMnO}_3$  bulk crystals<sup>11,94</sup> remains a topic for future investigations in  $\text{RMnO}_3$  thin films.

In addition to dimensionality scaling and heterostructure integration, thin-film realization of quantum oxide materials offers the

opportunity to use epitaxial constraints to further tune their functionality. The lattice mismatch with respect to the substrate can impart epitaxial strain in the thin film or induce interface defects, which affect both electronic and magnetic properties. In hexagonal  $\text{RMnO}_3$ , strain engineering can, in principle, be used to tune the improper ferroelectricity in terms of both domain configuration and polarization magnitude.<sup>96–98</sup> Although thin-film  $\text{RMnO}_3$  is often grown on substrates with large lattice mismatch exceeding 2% (see Fig. 9), the resulting epitaxial strain is not obvious.<sup>99</sup> Rather than inducing a coherently strained thin-film lattice, several other mechanisms are often at play that accommodate this mismatch. For example, misfit dislocations are frequently seen at the substrate–film interface, allowing bulk-like lattice constants to persist in the thin-film limit.<sup>49</sup> Structural or chemical mismatch at interfaces can additionally be accommodated through oxygen off-stoichiometry,<sup>62</sup> in-plane lattice rotation,<sup>95</sup> or interface reconstruction,<sup>88</sup> as shown in Fig. 11. It is possible that coherently strained epitaxial films could be achieved in hexagonal  $\text{RMnO}_3$  films if grown on substrates with smaller lattice mismatch. This, however, would require the design and development of new substrates that offer better compatibility with the family of hexagonal  $\text{ABO}_3$  materials.

An alternative route to achieve coherently strained heterostructures is demonstrated through the recent realization of mutual lattice matching between  $\text{RMnO}_3$  and  $\text{In}_2\text{O}_3$ -based transparent conducting layers such as indium-tin oxide (ITO). Straining the conducting layer to the  $\text{RMnO}_3$  lattice,<sup>81</sup> rather than vice versa, offers a new opportunity for epitaxial integration of hexagonal  $\text{ABO}_3$  into functional oxide-electronic heterostructures and superlattices [Figs. 12(a)–12(c)].

The layered structure of hexagonal  $\text{ABO}_3$  further distinguishes this class of oxides as prospective quantum materials. As already seen in Sec. I, the triangular sublattice of each half-unit-cell layer breaks inversion symmetry [see Fig. 1(b)]. Given the half-unit-cell layer-by-layer growth mode achieved by PLD,<sup>81</sup> the symmetry of the ultrathin thin-film system can be alternately controlled between preserved and broken inversion symmetry, purely based on either an even or odd total number of half-unit-cell layers.<sup>100</sup> This effect was demonstrated using *in situ* SHG<sup>101,102</sup> during hexagonal  $\text{RMnO}_3$  epitaxial growth [Fig. 12(d)]. Similar to 2D-layered van-der-Waals materials,<sup>103</sup> such layer-dependent symmetry control in thin films could, furthermore, be used to not only tune nonlinear optical responses but also may present an avenue to engineer, e.g., magnetoelectric, nonreciprocal, chiral, or topological effects in the general class of hexagonal  $\text{ABO}_3$  materials and their heterostructures.

Beyond the hexagonal manganites, the polar hexagonal  $P6_3cm$  phase has been achieved as bulk crystals for certain gallates ( $\text{AGaO}_3$ ,  $A = \text{Y, Er, Ho}$ <sup>104</sup>) and indates ( $\text{AlnO}_3$ ,  $A = \text{Y, Sm-Ho}$ ,<sup>105,106</sup>). The nonpolar  $P6_3/mmc$  hexagonal structure is furthermore the bulk-stable phase of  $\text{InFeO}_3$ .<sup>107,108</sup> Although thin films of hexagonal gallates and indates remain little explored so far, thin films of  $\text{InFeO}_3$  have been grown by PLD on both ZnO(0001) and Ta:SnO<sub>2</sub>-buffered  $\text{Al}_2\text{O}_3$  substrates.<sup>44,109</sup>  $\text{InFeO}_3$  films have been proposed as candidates for water-splitting and photoelectrode applications due to their beneficial bandgap placement.<sup>44</sup> Additionally, epitaxial  $\text{InFeO}_3$  has been used as structurally compatible nonpolar spacer layers in hexagonal  $\text{LuFeO}_3$ -based superlattices grown by oxide MBE.<sup>110</sup> The high volatility of indium and its sub-oxides<sup>111</sup> at the elevated temperatures required for crystallization of the hexagonal phase, however, renders the thin-film synthesis of the indium-based hexagonal compounds challenging;

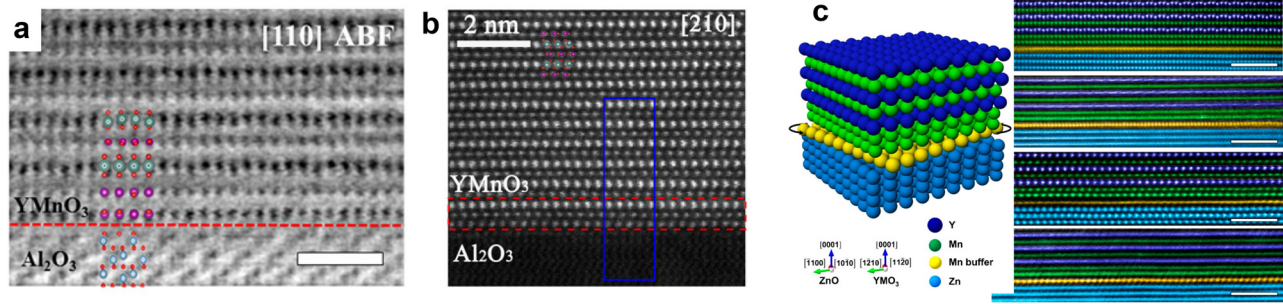


**FIG. 11.** Substrate–film interface reconstruction in hexagonal YMO<sub>3</sub> thin films visualized by HAADF-STEM. (a) and (b) Hexagonal YMO<sub>3</sub> films on sapphire substrates exhibit a double Mn-O layer at the interface that can host a charge ordered state of Mn<sup>3+</sup> and Mn<sup>2+</sup> ions. Reprinted with permission from Cheng *et al.*, *Sci. Adv.* **4**, eaar4298 (2018). Copyright 2018 Author(s), licensed under a Creative Commons Attribution 4.0 License.<sup>88</sup> (c) A triple Mn-O layer is formed between hexagonal YMO<sub>3</sub> and a ZnO(0001) substrate. The Mn-O layer closest to the substrate is reported to adopt a 5° in-plane rotation relative to both film and substrate, influencing the strain relaxation of the YMO<sub>3</sub> film. Reprinted with permission from Zhang *et al.*, *Nano Lett.* **21**, 6867–6874 (2021). Copyright 2021 American Chemical Society.<sup>95</sup>

such challenges can also be expected for hexagonal gallates given the similar volatility of gallium.

We note, however, that epitaxy of indates and gallates offers interesting opportunities to study the thin-film functional properties of hexagonal oxides in the absence of transition metal ions and magnetism on the B site. This enables, for example, isolating the physics of frustrated rare-earth magnetism on the hexagonal A-site lattice.<sup>33</sup> Moreover, in contrast to the transition-metal-based hexagonal ABO<sub>3</sub> oxides, which are mixed electronic and ionic conductors, the indates

and gallates are electronically insulating and could, thus, support pure oxygen-ion conductivity.

### V. EPITAXY OF METASTABLE HEXAGONAL ABO<sub>3</sub> COMPOUNDS

Thin-film epitaxy is also a powerful platform for exploring metastable hexagonal oxides. During crystal growth, the phase that is deposited minimizes the global energy of the system. The Gibbs free energy of formation for a crystal nucleating on a

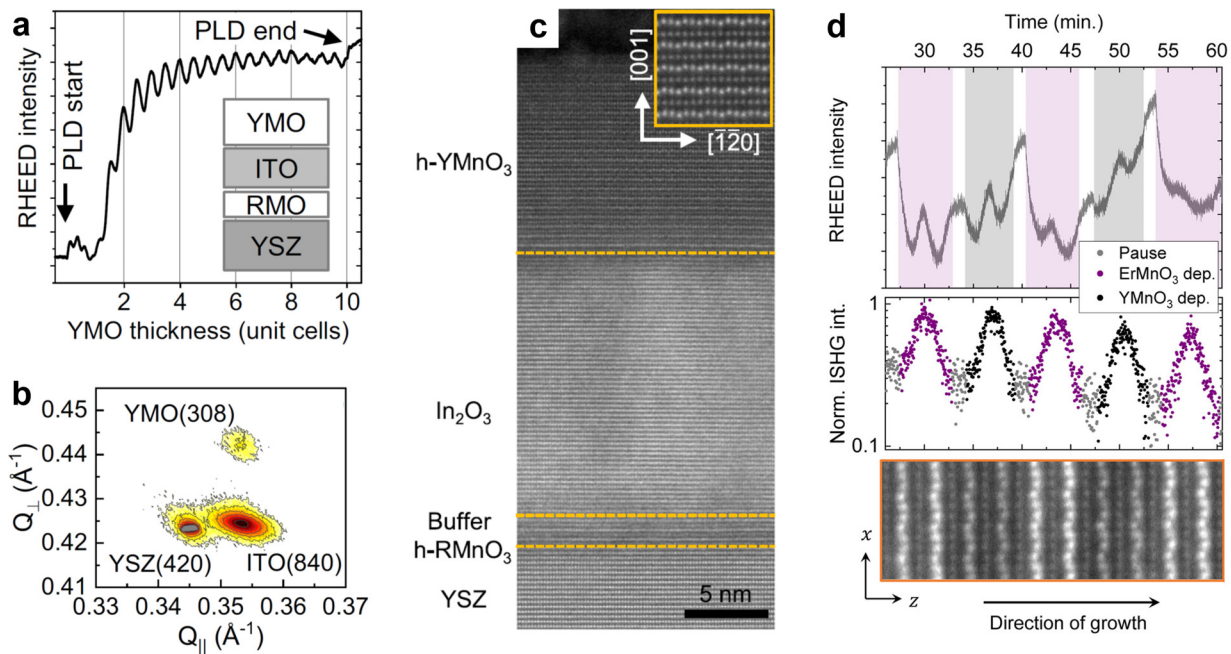


**FIG. 12.** Hexagonal RMnO<sub>3</sub> in epitaxial heterostructures. (a)–(c) Mutual lattice matching is achieved between YMO<sub>3</sub> and indium tin oxide (SnO<sub>2</sub>:In<sub>2</sub>O<sub>3</sub>, ITO) by inserting a buffer hexagonal RMnO<sub>3</sub> layer at the substrate interface to induce immediate strain relaxation. (a) RHEED oscillations indicating a layer-by-layer growth mode of YMO<sub>3</sub> in this heterostructure. (b) X-ray reciprocal space mapping shows matching of in-plane lattice parameters between ITO and YMO<sub>3</sub>, yet relaxed compared to the underlying YSZ substrate. (c) HAADF-STEM image of a similar heterostructure. (a)–(c) Reprinted with permission from Nordlander *et al.*, *Phys. Rev. Lett.* **4**, 124403 (2020). Copyright 2020 American Physical Society.<sup>81</sup> (d) A (YMO<sub>3</sub>)<sub>1</sub>(ErMnO<sub>3</sub>)<sub>1</sub> superlattice grown on YSZ(111). *In situ* optical second harmonic generation reveals the inversion-symmetry breaking of each half-unit-cell layer. Reprinted with permission from Nordlander *et al.*, *Nano Lett.* **21**, 2780–2785 (2021). Copyright 2021 American Chemical Society.<sup>100</sup>

substrate is comprised of a volume term, which will prefer the thermodynamically stable structure; a surface term, which is determined by the surface energy between the material and the substrate; and a stress term, which discourages the growth of highly stressed states. In the early stages of growth, the crystal nucleating on the substrate has a high surface-to-volume ratio, making the interface between the substrate and nucleating crystal a critical component in film growth. Because coherent crystalline interfaces require less energy to form than non-coherent ones, the film often adopts a structure which resembles the crystallographic structure of the substrate in epitaxial thin film growth. One of the powerful consequences of this minimization of interfacial energy between the substrate and film—known as epitaxial stabilization—is that a metastable crystal structure, not the lowest energy structure, can be grown.<sup>112,113</sup> By careful choice of substrate,<sup>58,114</sup> epitaxial stabilization enables the exploration of compounds in their metastable and nonequilibrium structures, opening the door to novel materials with new functionalities.

In the case of rare-earth manganites,  $R\text{MnO}_3$ , the ground-state structure depends largely on the  $R$ -site radius, as discussed in Sec. II. As the radius of the  $R$ -cation is decreased, the lower energy structure goes from orthorhombic (La–Dy) to hexagonal (Ho–Lu). The small energy difference in the bulk stable state near the crossover between orthorhombic and hexagonal (Fig. 6) can be overcome by epitaxial

stabilization. For example, Bosak *et al.* demonstrated that  $\text{EuMnO}_3$ ,  $\text{GdMnO}_3$ , and  $\text{DyMnO}_3$  could form the hexagonal phase by epitaxial stabilization on  $\text{YSZ}(111)$ ,<sup>67</sup> and that  $\text{HoMnO}_3$ ,  $\text{TmMnO}_3$  and  $\text{LuMnO}_3$  could form the orthorhombic phase using  $\text{LaAlO}_3(001)$  or  $\text{SrTiO}_3(001)$  substrates<sup>115</sup> (Table II).

Notably, unlike the manganites, there are no known bulk-stable hexagonal ferrites besides  $\text{InFeO}_3$ .<sup>107,108</sup> Instead, the  $R\text{FeO}_3$  ferrites are usually orthorhombic in their ground state, due to the crystal field splitting of the orbitals as discussed in Sec. II. However, many of the  $R\text{FeO}_3$  structures have been epitaxially stabilized for  $R$  with smaller cation radius (Y, Sc, Eu, and Tb–Lu), as summarized in Table II. In addition to epitaxial stabilization, “stromataxic stabilization” can be used to further increase the number of compounds which can be synthesized in the thin film form.<sup>51</sup> Garten *et al.* showed that by using sequential atomic layering they could form hexagonal  $\text{ScFeO}_3$  with the  $\text{YMnO}_3$ -like structure. In the same growth conditions, co-deposition of scandium and iron yielded the bixbyite polymorph. Stromataxic stabilization is a powerful technique that could likely be used to construct other metastable hexagonal oxides, beyond those which can be constructed by epitaxial stabilization alone.

Stabilizing these hexagonal  $\text{AFeO}_3$  ferrites opens the door to further engineering their ferroelectric, magnetic, and multiferroic properties. Here, we will focus on  $\text{LuFeO}_3$ , since it has seen as a recent surge in interest—for an overview of the other  $\text{AFeO}_3$  compositions, refer to

**TABLE II.** Summary of the  $R\text{MnO}_3$  and  $R\text{FeO}_3$  structures where  $R$  = rare earth, Sc, In, and Y. The bulk-stable phase is listed in addition to the structures which can be epitaxially stabilized on the listed substrate or template. o, h, and b refer to orthorhombic, hexagonal, and bixbyite, respectively.

	Mn					Fe				
	Stable structure		Epitaxially stabilized			Stable structure		Epitaxially stabilized		
La	o <sup>55,116</sup>	$Pbnm$				o <sup>117</sup>	$Pbnm$			
Ce	o <sup>118</sup>	$Pbnm$				o <sup>119</sup>	$Pnma$			
Pr	o <sup>120</sup>	$Pbnm$				o <sup>117</sup>	$Pbnm$			
Nd	o <sup>120,121</sup>	$Pbnm$				o <sup>117</sup>	$Pbnm$			
Sm	o <sup>55,121</sup>	$Pnma$				o <sup>117</sup>	$Pbnm$			
Eu	o <sup>120,121</sup>	$Pbnm$	h <sup>67</sup>	$P6_3cm$	$\text{YSZ}(111)$	o <sup>117</sup>	$Pbnm$	h <sup>122</sup>	$P6_3cm$	$\text{YSZ}(111)$
Gd	o <sup>121</sup>	$Pnma$	h <sup>67</sup>	$P6_3cm$	$\text{YSZ}(111)$	o <sup>117</sup>	$Pbnm$			
Tb	o <sup>123</sup>	$Pnma$				o <sup>124</sup>	$Pbnm$	h <sup>14</sup>	$P6_3cm$	$\text{YSZ}(111)$
Dy	o <sup>55,120,121</sup>	$Pbnm$	h <sup>67</sup>	$P6_3cm$	$\text{YSZ}(111)$	o <sup>124</sup>	$Pbnm$	h <sup>14</sup>	$P6_3cm$	$\text{YSZ}(111)$
Ho	h <sup>5,121</sup>	$P6_3cm$	o <sup>115</sup>	$Pnma$	$\text{LaAlO}_3(001)$ $\text{SrTiO}_3(001)$	o <sup>124</sup>	$Pbnm$	h <sup>14</sup>	$P6_3cm$	$\text{YSZ}(111)$
Er	h <sup>5,55,125</sup>	$P6_3cm$				o <sup>124</sup>	$Pbnm$	h <sup>122</sup>	$P6_3cm$	$\text{YSZ}(111)$
Tm	h <sup>5,121</sup>	$P6_3cm$	o <sup>115</sup>	$Pnma$	$\text{LaAlO}_3(001)$ $\text{SrTiO}_3(001)$	o <sup>124</sup>	$Pbnm$	h <sup>122</sup>	$P6_3cm$	$\text{YSZ}(111)$
Yb	h <sup>5,55,121</sup>	$P6_3cm$				o <sup>124</sup>	$Pbnm$	h <sup>122</sup>	$P6_3cm$	$\text{YSZ}(111)$
Lu	h <sup>5,121</sup>	$P6_3cm$	o <sup>115</sup>	$Pnma$	$\text{LaAlO}_3(001)$ $\text{SrTiO}_3(001)$	o <sup>124</sup>	$Pbnm$	h <sup>122,126</sup>	$P6_3cm$	$\text{YSZ}(111)$ $\text{Al}_2\text{O}_3(0001)$ $\text{Fe}_3\text{O}_4(111)$
Sc	h <sup>127</sup>	$P6_3cm$				b <sup>128</sup>	$Ia\bar{3}$	h <sup>114</sup>	$P6_3cm$	$\text{Al}_2\text{O}_3(0001)$
In	h <sup>129</sup>	$P6_3cm$				h <sup>108</sup>	$P6_3/mmc$			
Y	h <sup>5,55</sup>	$P6_3cm$	o	$Pnma$	$\text{LaAlO}_3(001)$ $\text{SrTiO}_3(001)$	o <sup>117</sup>	$Pbnm$	h <sup>130</sup>	$P6_3cm$	$\text{Pt}(111)$

an earlier review of hexagonal ferrites.<sup>131</sup> While  $\text{LuFeO}_3$  is stable in the orthorhombic structure in the bulk, it can be epitaxially stabilized to be isostructural to  $\text{YMnO}_3$ ,<sup>122</sup> as shown in Table II. In addition to YSZ(111),<sup>122,132</sup>  $\text{LuFeO}_3$  has been epitaxially stabilized on the basal plane of  $\text{Al}_2\text{O}_3$ ,<sup>16</sup> Ir(111), Pt(111),<sup>133</sup>  $\text{Fe}_3\text{O}_4$ (111),<sup>126</sup> ITO<sup>134</sup> and GaN.<sup>135</sup> Figures 13(a) and 13(b) show high-resolution HAADF-STEM images of epitaxially stabilized  $\text{LuFeO}_3$  synthesized by MOCVD [Fig. 13(a)] and MBE [Fig. 13(b)]. This hexagonal structure is an improper ferroelectric with  $P6_3cm$  symmetry (similar to what was discussed in Sec. IV) with a polarization of  $6.5 \mu\text{C}/\text{cm}^2$  (Ref. 133) and a Curie temperature around 1020 K.<sup>16</sup> The switching of the polarization by piezoresponse force microscopy<sup>15</sup> is shown in Fig. 13(c). The hexagonal symmetry of the structure produces a magnetically frustrated system, which results in two-dimensional arrangements of spins in the iron planes, as shown in Fig. 2, resulting in an antiferromagnet. Below approximately 145 K, the spins cant in the [0001] direction, producing a net magnetic moment, displayed in Fig. 13(d).<sup>16,132</sup>

Due to the simultaneous existence of ferroelectricity and a weak ferromagnetic moment,  $\text{LuFeO}_3$  is a promising candidate for multiferroic materials. In particular, compared to the hexagonal manganites, the hexagonal ferrites promise higher magnetic transition temperatures and magnetoelectric coupling due to the additional occupied orbital<sup>17</sup> (the five  $d$  electrons in  $\text{Fe}^{+3}$  half fill each of the orbitals in Fig. 5). While  $\text{LuFeO}_3$  itself only has a net magnetic moment at cryogenic temperatures,  $\text{LuFeO}_3$  can be synthesized in a

superlattice with other materials in an effort to enhance the magnetism. The first attempts included cobalt-doped  $\text{LuFeO}_3$ ,<sup>136</sup> depicted in Fig. 14(a). It was found that these materials showed a decrease in the magnetic ordering temperatures with respect to  $\text{LuFeO}_3$  and  $\text{LuFe}_{2-x}\text{Co}_x\text{O}_4$ . More recently,  $\text{LuFeO}_3$  was grown in a superlattice structure with formula-unit-thick layers of  $\text{LuFe}_2\text{O}_4$ , a hexagonal ferrite with a 240 K ferrimagnetic transition temperature, to create a room-temperature multiferroic.<sup>50</sup> In these superlattices shown in Fig. 14(b), the ferroelectric distortion from the  $\text{LuFeO}_3$  reduced the magnetic frustration in the  $\text{LuFe}_2\text{O}_4$ , increasing the magnetic transition temperature to 281 K. The material further demonstrated electric field control of magnetism—creating a magnetoelectric multiferroic (Fig. 15). This opens doors to the new engineering of multiferroic materials based on these epitaxially stabilized, improper ferroelectrics. We further note that  $\text{LuFeO}_3$  can be epitaxially stabilized on intergrown spinel  $\text{Fe}_3\text{O}_4$  (magnetite).<sup>126</sup> The very high magnetic ordering temperature of  $\text{Fe}_3\text{O}_4$  and other spinel compounds could provide a pathway to create a multiferroic with simultaneous transitions well above room temperature.

In addition to their coupled electric and magnetic orders, hexagonal ferrites, like the hexagonal manganites, host topological defects such as their ferroelectric domain walls and vortices where six ferroelectric domains come to a point. The superlattice construction of  $(\text{LuFeO}_3)_m/\text{LuFe}_2\text{O}_4$  provides an avenue to manipulate these topological textures in hexagonal ferroelectrics.<sup>110</sup> As the confinement of the ferroelectric layer

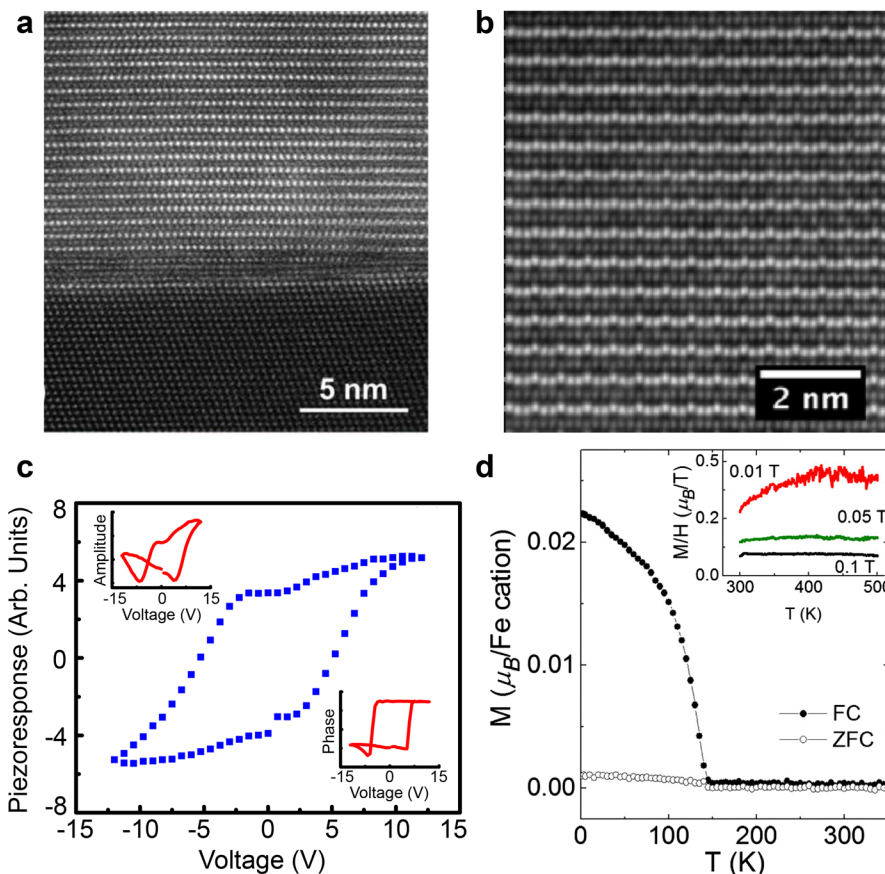


**FIG. 13.** Characterization of epitaxially stabilized  $\text{LuFeO}_3$  thin films. (a) HAADF STEM micrograph of a  $\text{LuFeO}_3$  thin film on YSZ(111). Republished with permission from Akbashev *et al.*, *CrystEngComm* **14**, 5373–5376 (2012). Copyright 2012 The Royal Society of Chemistry.<sup>36</sup> (b) HAADF STEM micrograph showing the trimerization of the brighter lutetium atoms characteristic of the  $P6_3cm$  structure. (c) PFM measurement of  $\text{LuFeO}_3/\text{Pt}/\text{Al}_2\text{O}_3$  showing a hysteresis loop with phase and amplitude curves inset. Reprinted with permission from Wang *et al.*, *Phys. Rev. Lett.* **110**, 237601 (2013). Copyright 2013 American Physical Society.<sup>15</sup> (d) Magnetization vs temperature in a 0.01 T field applied out of plane of a 250 nm film of  $\text{LuFeO}_3$  on YSZ(111) indicating a weak ferromagnetic transition at 143 K with inset high temperature behavior at various applied fields. (b) and (d) Reprinted with permission from Disseler *et al.*, *Phys. Rev. Lett.* **114**, 217602 (2015). Copyright 2015 American Physical Society.<sup>16</sup>

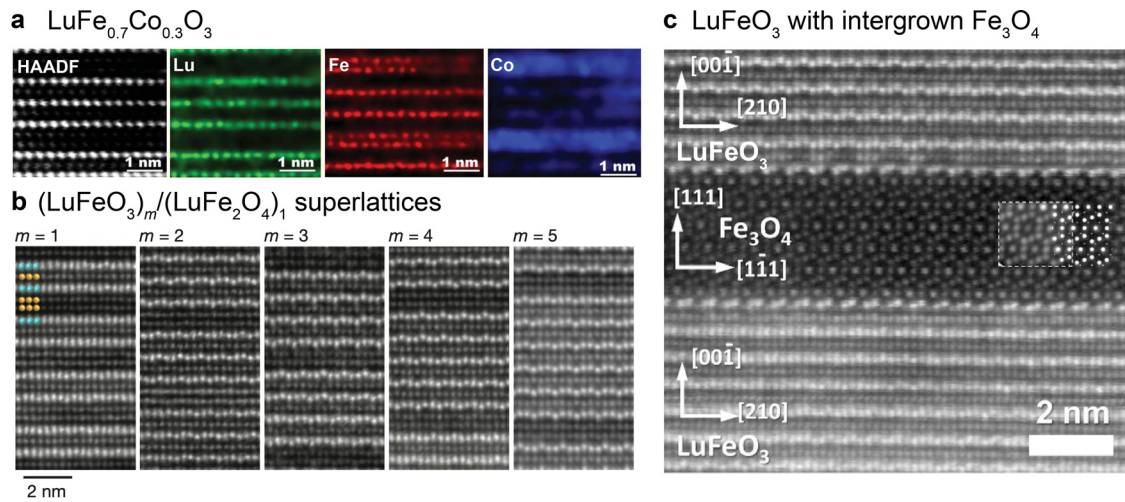


**FIG. 14.** STEM micrographs of  $\text{LuFeO}_3$  thin films combined with other materials. (a) HAADF STEM and atomic resolution EDS of a small region of cobalt-doped  $\text{LuFeO}_3$ , nominally  $\text{LuFe}_{0.7}\text{Co}_{0.3}\text{O}_3$ . Republished with permission from Akbashev *et al.*, *CrystEngComm* **14**, 5373–5376 (2012). Copyright 2012 The Royal Society of Chemistry.<sup>36</sup> (b) HAADF-STEM micrographs of the  $m = 1$ –5 members of the  $(\text{LuFeO}_3)_m/(\text{LuFe}_2\text{O}_4)_1$  superlattice series imaged along the  $\text{LuFeO}_3$  [100] zone axis. The leftmost image shows the position of lutetium (teal) and iron (yellow) atomic columns. Reprinted with permission from Mundy *et al.*, *Nature* **537**, 523–527 (2016). Copyright 2016 Springer Nature.<sup>50</sup> (c) HAADF-STEM micrograph of an iron-rich  $\text{LuFeO}_3$  film with ingrown epitaxial  $\text{Fe}_3\text{O}_4$  nanolayers. The inset shows a HAADF-STEM simulation of  $\text{Fe}_3\text{O}_4$  along with white dots that mark the imaged iron positions. Reprinted with permission from Akbashev *et al.*, *Sci. Rep.* **2**, 672 (2012). Copyright 2012 Springer Nature.<sup>126</sup>

is increased, the material goes from stabilizing charged domain walls with threefold and fivefold fractional vortices, to having irregular domains with neutral domain walls. As the confinement approaches one monolayer of  $\text{LuFeO}_3$ , the ferroelectricity is suppressed—reminiscent of the ferroelectric to paraelectric transition with temperature.

## VI. OUTLOOK

The hexagonal  $\text{ABO}_3$  materials are a rich class of quantum materials. In addition to the well-studied multiferroicity in the hexagonal

manganites, there has been recent interest in stabilizing the elusive quantum spin liquid<sup>33</sup> and predicted topological semimetal states<sup>47</sup> and unconventional superconductivity.<sup>36</sup> Thin-film epitaxy provides a powerful platform for both studying these materials at the fundamental limits<sup>49</sup> as well as potentially stabilizing new materials. More recent work has used precise chemical layering<sup>51</sup> to access compounds that were not accessible with epitaxial stabilization alone. Combined, thin-film epitaxy should allow additional emergent phenomena to be uncovered in the hexagonal oxides.

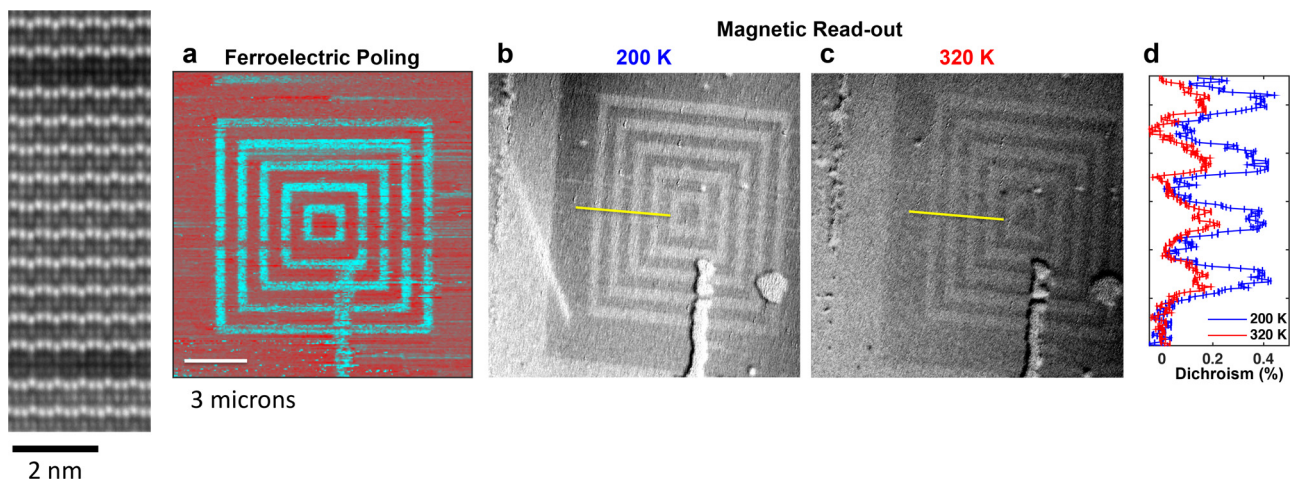


**FIG. 15.** Magneto-electric coupling in  $(\text{LuFeO}_3)_m/\text{LuFe}_2\text{O}_4$  superlattices. Left, a HAADF-STEM micrograph of a  $(\text{LuFeO}_3)_9/\text{LuFe}_2\text{O}_4$  superlattice showing one period of the layered structure. (a) An out-of-plane PFM image at 300 K of an electrically poled region of the  $m = 9$  superlattice film showing a pattern of up (teal) and down (red)  $c$ -axis polarized domains. (b) An XMCD PEEM image of the  $\text{Fe } L_3$  edge of the poled region in (a) taken at 200 K. (c) The same image as (b) collected at 320 K. (d) Line profiles of the XMCD signal along the yellow lines in (b) and (c). The correspondence between the PFM and PEEM images demonstrates the coupling between improper ferroelectricity and ferrimagnetism in the film. Reprinted with permission from Mundy *et al.*, *Nature* **537**, 523–527 (2016). Copyright 2016 Springer Nature.<sup>50</sup>

## ACKNOWLEDGMENTS

The authors would like to thank Hena Das and EliseAnne Koskelo for their fruitful discussions. This work was supported by the Air Force Office of Scientific Research (MURI Grant No. FA9550-21-1-0429). J.A.M acknowledges the support from the Packard Foundation and Gordon and Betty Moore Foundation's EPIQS Initiative (Grant No. GBMF6760). J.N. acknowledges the support from the Swiss National Science Foundation under Project No. P2EZP2\_195686.

## AUTHOR DECLARATIONS

### Conflict of Interest

The authors have no conflicts to disclose.

### Author Contributions

**Johanna Nordlander:** Data curation (equal); Visualization (equal); Writing – original draft (lead); Writing – review and editing (lead). **Margaret A Anderson:** Data curation (equal); Visualization (equal); Writing – original draft (equal); Writing – review and editing (equal). **Charles M Brooks:** Visualization (equal); Writing – original draft (equal); Writing – review and editing (equal). **Megan E Holtz:** Data curation (equal); Visualization (equal); Writing – original draft (equal); Writing – review and editing (equal). **Julia Mundy:** Data curation (equal); Supervision (lead); Visualization (equal); Writing – original draft (equal); Writing – review and editing (equal).

## DATA AVAILABILITY

Data sharing is not applicable to this article as no new data were created or analyzed in this study.

## APPENDIX: A NOTE ON HEXAGONAL GEOMETRY

The effective hexagonal in-plane lattice parameter of a (111)-oriented cubic crystal depends on the type of cubic structure the material forms. The simplest structure is the simple cube. For a crystal with cations on the corners of a cube, the (111) lattice parameter is given by the length of the face diagonal of the cube:

$$a_{hex} = a_{SC}\sqrt{2}.$$

Materials that follow this formula include cubic perovskites (e.g., SrTiO<sub>3</sub>, KTaO<sub>3</sub>, and LaAlO<sub>3</sub>). Most of the common substrates and bottom electrode materials considered in this review have a face-centered cubic (FCC) structure. For this structure, the hexagonal lattice parameter is given by (1/2) of the face diagonal of the cubic unit cell:

$$a_{hex} = \frac{a_{FCC}\sqrt{2}}{2}.$$

Various single elements (e.g., Ir, Pt, Pd, Ag, Si) crystallize in an FCC lattice. Spinel (e.g., MgAl<sub>2</sub>O<sub>4</sub>) and rock salt-type structures (e.g., MgO) also follow the FCC formula. Other materials with an FCC-type configuration include 3C-SiC, CaF<sub>2</sub>, and yttria-stabilized zirconia (YSZ). Some elements crystallize as a body-centered cubic (BCC)

lattice (e.g., Cr, Mn, Fe, Mo). The hexagonal lattice parameter for this structure is the length of the face diagonal, just as in the simple cubic case, because the central atom lies slightly out of the (111) plane that includes three corner atoms. For the more complicated bixbyite structure, the true (111) lattice parameter follows the simple cubic formula ( $a_{hex} = a_{bixbyite}\sqrt{2}$ ). However, there are cations in a slightly distorted hexagonal lattice with average spacing  $a_{hex}/4$ . For this reason, the hexagonal lattice parameter of the bixbyite compound In<sub>2</sub>O<sub>3</sub> is reported as 3.58 Å above while the cubic lattice parameter is 10.12 Å, giving 14.31 Å between identical lattice sites in the (111) plane. Other bixbyite materials include R<sub>2</sub>O<sub>3</sub>, Y<sub>2</sub>O<sub>3</sub>, and Mn<sub>2</sub>O<sub>3</sub>.

Lattice matching between hexagonal crystals is more complicated than that of cubic or orthorhombic structures. While both structures can accommodate matching between crystals with integer ratios between their lattice parameters (e.g.,  $a$  and  $2a$ ), hexagonal films can also incorporate scaling factors like  $\frac{2}{3}$  or  $\frac{4}{3}$  as well as a 30° rotation between the film and substrate. The rotation effectively scales the lattice parameter by  $\sqrt{3}$ . This possible rotation, along with a scarcity of substrates with proper lattice parameters, complicates studies of strain engineering in hexagonal thin films. As with cubic thin films, the lattice mismatch between substrate and film is quantified as

$$\text{lattice mismatch (\%)} = \frac{a_{sub} - a_{film}}{a_{film}} \times 100.$$

For many materials, this simple formula can accurately predict which substrates and films are compatible and how they will align. However, this calculation is imperfect. Especially for large lattice mismatch, the

**TABLE III.** Equivalent hexagonal lattice parameters for the substrate materials considered in Fig. 9.

Compound	Orientation	Hexagonal lattice constant (Å)	30° Rotated lattice constant (Å)
$\alpha$ -Al <sub>2</sub> O <sub>3</sub>	(0001)	4.76	8.24
YSZ	(111)	3.64	6.30
GaN	(0001)	3.19	5.52
SCAM	(0001)	3.25	5.62
4H-SiC	(0001)	3.07	5.32
ZnO	(0001)	3.25	5.63
Graphite	(0001)	2.46	4.26
In <sub>2</sub> O <sub>3</sub>	(111)	14.31 (3.58)	24.79 (6.20)
CaF <sub>2</sub>	(111)	3.86	6.69
KTaO <sub>3</sub>	(111)	5.64	9.77
LaAlO <sub>3</sub>	(111)	5.37	9.30
MgAl <sub>2</sub> O <sub>4</sub>	(111)	5.71	9.90
CoFe <sub>2</sub> O <sub>4</sub>	(111)	3.67	6.36
MgO	(111)	2.98	5.16
3C-SiC	(111)	3.08	5.33
SrTiO <sub>3</sub>	(111)	5.52	9.56
Pt	(111)	2.78	4.82
Pd	(111)	2.75	4.76
Ir	(111)	2.72	4.70
Si	(111)	3.84	6.65

TABLE IV. Lattice parameters of known hexagonal  $ABO_3$  compounds.

Film	Geometry	Lattice constant (Å)	30° Rotated lattice constant (Å)	Reference
YMnO <sub>3</sub>	Bulk	6.13		5
GdMnO <sub>3</sub>	Thin film	6.30		137
HoMnO <sub>3</sub>	Bulk	6.14		5
ErMnO <sub>3</sub>	Bulk	6.12		5
TmMnO <sub>3</sub>	Bulk	6.06		5
YbMnO <sub>3</sub>	Bulk	6.06		5
LuMnO <sub>3</sub>	Bulk	6.04		5
TbMnO <sub>3</sub>	Thin film	6.27		74
DyMnO <sub>3</sub>	Bulk	6.19		138
LuFeO <sub>3</sub>	Bulk	5.97		122 and 126
LuFe <sub>2</sub> O <sub>4</sub>	Bulk	3.43	5.96	139
DyFeO <sub>3</sub>	Thin film	6.24		41
DyFe <sub>2</sub> O <sub>4</sub>	Thin film	3.54	6.13	140
YbFeO <sub>3</sub>	Thin film	3.46	5.99	141
ErFeO <sub>3</sub>	Thin film	6.05–6.09		122 and 142
ScFeO <sub>3</sub>	Thin film	5.72		143
TmFeO <sub>3</sub>	Thin film	6.02		122
YFeO <sub>3</sub>	Bulk	3.51	6.08	144
InFeO <sub>3</sub>	Thin film	3.32	5.75	109
InFe <sub>2</sub> O <sub>4</sub>	Thin film	3.36	5.82	109
InMnO <sub>3</sub>	Bulk	5.88		145
YInO <sub>3</sub>	Bulk	6.27		146
HoInO <sub>3</sub>	Bulk	6.27		146
DyInO <sub>3</sub>	Bulk	6.30		146
TbInO <sub>3</sub>	Bulk	6.32		146
GdInO <sub>3</sub>	Bulk	6.35		146
EuInO <sub>3</sub>	Bulk	6.38		146
SmInO <sub>3</sub>	Bulk	6.42		146
YGaO <sub>3</sub>	Bulk	6.07		147
InGaO <sub>3</sub>	Bulk	3.31	5.73	145

difference in lattice parameters does not tell the whole story. The exact termination of the substrate and structure of the sublattice—the positions and identities of atoms that lie within the cations that define the hexagonal unit cell—can change how the substrate and film will align to reduce energy at the interface. Furthermore, the tendency of hexagonal crystals to adopt a 30° rotation or unusual scaling factor between film and substrate complicates the quantification of the lattice mismatch because the alignment can dramatically affect the effective lattice parameter of the substrate.

We tabulate the lattice parameters used for substrate and film materials (Tables III and IV, respectively) shown in Fig. 9.

## REFERENCES

- H. Y. Hwang, Y. Iwasa, M. Kawasaki, B. Keimer, N. Nagaosa, and Y. Tokura, “Emergent phenomena at oxide interfaces,” *Nat. Mater.* **11**, 103–113 (2012).
- D. G. Schlom, L.-Q. Chen, X. Pan, A. Schmehl, and M. A. Zurbuchen, “A thin film approach to engineering functionality into oxides,” *J. Am. Ceram. Soc.* **91**, 2429–2454 (2008).

- J. Mannhart and D. G. Schlom, “Oxide interfaces—an opportunity for electronics,” *Science* **327**, 1607–1611 (2010).
- L. T. Nguyen and R. Cava, “Hexagonal perovskites as quantum materials,” *Chem. Rev.* **121**, 2935–2965 (2020).
- H. Yakel, W. Koehler, E. Bertaut, and E. Forrat, “On the crystal structure of the manganese(III) trioxides of the heavy lanthanides and yttrium,” *Acta Crystallogr.* **16**, 957–962 (1963).
- M. Lilienblum, T. Lottermoser, S. Manz, S. M. Selbach, A. Cano, and M. Fiebig, “Ferroelectricity in the multiferroic hexagonal manganites,” *Nat. Phys.* **11**, 1070–1073 (2015).
- B. B. Van Aken, T. T. Palstra, A. Filippetti, and N. A. Spaldin, “The origin of ferroelectricity in magnetoelectric YMnO<sub>3</sub>,” *Nat. Mater.* **3**, 164–170 (2004).
- C. J. Fennie and K. M. Rabe, “Ferroelectric transition in YMnO<sub>3</sub> from first principles,” *Phys. Rev. B* **72**, 100103 (2005).
- E. Bertaut, R. Pauthenet, and M. Mercier, “Magnetic properties and structures of yttrium manganite,” *Phys. Lett.* **7**, 110–111 (1963).
- Z. J. Huang, Y. Cao, Y. Y. Sun, Y. Y. Xue, and C. W. Chu, “Coupling between the ferroelectric and antiferromagnetic orders in YMnO<sub>3</sub>,” *Phys. Rev. B* **56**, 2623–2626 (1997).
- M. Fiebig, T. Lottermoser, D. Fröhlich, A. V. Goltsev, and R. V. Pisarev, “Observation of coupled magnetic and electric domains,” *Nature* **419**, 818–820 (2002).
- T. Lottermoser, T. Lonkai, U. Amann, D. Hohlwein, J. Ihringer, and M. Fiebig, “Magnetic phase control by an electric field,” *Nature* **430**, 541–544 (2004).
- B. Lorenz, “Hexagonal manganites-(RMnO<sub>3</sub>): Class (I) multiferroics with strong coupling of magnetism and ferroelectricity,” *ISRN Condens. Matter Phys.* **2013**, 497073.
- A. Akbashev, A. Semisalova, N. Perov, and A. Kaul, “Weak ferromagnetism in hexagonal orthoferrites RFeO<sub>3</sub> (R = Lu, Er-Tb),” *Appl. Phys. Lett.* **99**, 122502 (2011).
- W. Wang, J. Zhao, W. Wang, Z. Gai, N. Balke, M. Chi, H. N. Lee, W. Tian, L. Zhu, X. Cheng, D. J. Keavney, J. Yi, T. Z. Ward, P. C. Snijders, H. M. Christen, W. Wu, J. Shen, and X. Xu, “Room-temperature multiferroic hexagonal LuFeO<sub>3</sub> films,” *Phys. Rev. Lett.* **110**, 237601 (2013).
- S. M. Disseler, J. A. Borchers, C. M. Brooks, J. A. Mundy, J. A. Moyer, D. A. Hillsberry, E. L. Thies, D. A. Tenne, J. Heron, M. E. Holtz, J. D. Clarkson, G. M. Stiehl, P. Schiffer, D. A. Muller, D. G. Schlom, and W. D. Ratcliff, “Magnetic structure and ordering of multiferroic hexagonal LuFeO<sub>3</sub>,” *Phys. Rev. Lett.* **114**, 217602 (2015).
- H. Das, A. L. Wysocki, Y. Geng, W. Wu, and C. J. Fennie, “Bulk magnetoelectricity in the hexagonal manganites and ferrites,” *Nat. Commun.* **5**, 2998 (2014).
- S. Manapatruni, D. E. Nikonov, C.-C. Lin, T. A. Gosavi, H. Liu, B. Prasad, Y.-L. Huang, E. Bonturim, R. Ramesh, and I. A. Young, “Scalable energy-efficient magnetoelectric spin-orbit logic,” *Nature* **565**, 35–42 (2019).
- T. Choi, Y. Horibe, H. Yi, Y. J. Choi, W. Wu, and S.-W. Cheong, “Insulating interlocked ferroelectric and structural antiphase domain walls in multiferroic YMnO<sub>3</sub>,” *Nat. Mater.* **9**, 253–258 (2010).
- D. Meier, J. Seidel, A. Cano, K. Delaney, Y. Kumagai, M. Mostovoy, N. A. Spaldin, R. Ramesh, and M. Fiebig, “Anisotropic conductance at improper ferroelectric domain walls,” *Nat. Mater.* **11**, 284–288 (2012).
- J. A. Mundy, J. Schaab, Y. Kumagai, A. Cano, M. Stengel, I. P. Krug, D. M. Gottlob, H. Doğanay, M. E. Holtz, R. Held, Z. Yan, E. Bourret, C. M. Schneider, D. G. Schlom, D. A. Muller, R. Ramesh, N. A. Spaldin, and D. Meier, “Functional electronic inversion layers at ferroelectric domain walls,” *Nat. Mater.* **16**, 622–627 (2017).
- S. M. Griffin, M. Lilienblum, K. T. Delaney, Y. Kumagai, M. Fiebig, and N. A. Spaldin, “Scaling behavior and beyond equilibrium in the hexagonal manganites,” *Phys. Rev. X* **2**, 041022 (2012).
- S.-Z. Lin, X. Wang, Y. Kamiya, G.-W. Chern, F. Fan, D. Fan, B. Casas, Y. Liu, V. Kiryukhin, W. H. Zurek, C. D. Batista, and S.-W. Cheong, “Topological defects as relics of emergent continuous symmetry and Higgs condensation of disorder in ferroelectrics,” *Nat. Phys.* **10**, 970–977 (2014).
- Q. N. Meier, M. Lilienblum, S. M. Griffin, K. Conder, E. Pomjakushina, Z. Yan, E. Bourret, D. Meier, F. Lichtenberg, E. K. H. Salje, N. A. Spaldin, M. Fiebig, and A. Cano, “Global formation of topological defects in the multiferroic hexagonal manganites,” *Phys. Rev. X* **7**, 041014 (2017).

- <sup>25</sup>Q. N. Meier, A. Stucky, J. Teyssier, S. M. Griffin, D. van der Marel, and N. A. Spaldin, "Manifestation of structural higgs and goldstone modes in the hexagonal manganites," *Phys. Rev. B* **102**, 014102 (2020).
- <sup>26</sup>M. Norman, "Colloquium: Herbertsmithite and the search for the quantum spin liquid," *Rev. Mod. Phys.* **88**, 041002 (2016).
- <sup>27</sup>Y. Kasahara, T. Ohnishi, Y. Mizukami, O. Tanaka, S. Ma, K. Sugii, N. Kurita, H. Tanaka, J. Nasu, Y. Motome, T. Shibauchi, and Y. Matsuda, "Majorana quantization and half-integer thermal quantum Hall effect in a Kitaev spin liquid," *Nature* **559**, 227–231 (2018).
- <sup>28</sup>V. Kataev, A. Möller, U. Löw, W. Jung, N. Schittner, M. Kriener, and A. Freimuth, "Structural and magnetic properties of the new low-dimensional spin magnet  $\text{InCu}_{2/3}\text{V}_{1/3}\text{O}_3$ ," *J. Magn. Mater.* **290**, 310–313 (2005).
- <sup>29</sup>Y. Yan, Z. Li, T. Zhang, X. Luo, G. Ye, Z. Xiang, P. Cheng, L.-J. Zou, and X. Chen, "Magnetic properties of the doped spin-1/2 honeycomb-lattice compound  $\text{In}_3\text{Cu}_2\text{VO}_9$ ," *Phys. Rev. B* **85**, 085102 (2012).
- <sup>30</sup>D.-Y. Liu, Y. Guo, X.-L. Zhang, J.-L. Wang, Z. Zeng, H.-Q. Lin, and L.-J. Zou, "Interlayer magnetic-frustration-driven quantum spin disorder in the honeycomb compound  $\text{In}_3\text{Cu}_2\text{VO}_9$ ," *Europhys. Lett.* **103**, 47010 (2013).
- <sup>31</sup>W. Wu, M. M. Scherer, C. Honerkamp, and K. L. Hur, "Correlated Dirac particles and superconductivity on the honeycomb lattice," *Phys. Rev. B* **87**, 094521 (2013).
- <sup>32</sup>D. A. Vander Griend, S. Boudin, V. Caignaert, K. R. Poeppelmeier, Y. Wang, V. P. Dravid, M. Azuma, M. Takano, Z. Hu, and J. D. Jorgensen, " $\text{La}_4\text{Cu}_3\text{MoO}_{12}$ : A novel cuprate with unusual magnetism," *J. Am. Chem. Soc.* **121**, 4787–4792 (1999).
- <sup>33</sup>L. Clark, G. Sala, D. D. Maharaj, M. B. Stone, K. S. Knight, M. T. Telling, X. Wang, X. Xu, J. Kim, Y. Li, S.-W. Cheong, and B. D. Gaulin, "Two-dimensional spin liquid behaviour in the triangular-honeycomb antiferromagnet  $\text{TbInO}_3$ ," *Nat. Phys.* **15**, 262–268 (2019).
- <sup>34</sup>J. A. Mundy, Q. Mao, C. M. Brooks, D. G. Schlom, and D. A. Muller, "Atomic-resolution chemical imaging of oxygen local bonding environments by electron energy loss spectroscopy," *Appl. Phys. Lett.* **101**, 042907 (2012).
- <sup>35</sup>S. Remsen and B. Dabrowski, "Synthesis and oxygen storage capacities of hexagonal  $\text{Dy}_{1-x}\text{Y}_x\text{MnO}_{3+\delta}$ ," *Chem. Mater.* **23**, 3818–3827 (2011).
- <sup>36</sup>J. Hu, C. Le, and X. Wu, "Predicting unconventional high-temperature superconductors in trigonal bipyramidal coordinations," *Phys. Rev. X* **5**, 041012 (2015).
- <sup>37</sup>X. Huang, T. R. Paudel, S. Dong, and E. Y. Tsybal, "Hexagonal rare-earth manganites as promising photovoltaics and light polarizers," *Phys. Rev. B* **92**, 125201 (2015).
- <sup>38</sup>H. Han, S. Song, J. H. Lee, K. J. Kim, G. W. Kim, T. Park, and H. M. Jang, "Switchable photovoltaic effects in hexagonal manganite thin films having narrow band gaps," *Chem. Mater.* **27**, 7425–7432 (2015).
- <sup>39</sup>J. Li, A. W. Sleight, and M. Subramanian, "Determination of the local environment of  $\text{Mn}^{3+}$  and  $\text{In}^{3+}$  in the  $\text{YInO}_3$ - $\text{YMnO}_3$  solid solution, which exhibits an intense blue color," *Chem. Mater.* **28**, 6050–6053 (2016).
- <sup>40</sup>S. H. Skjærvø, E. T. Wefring, S. K. Nesdal, N. H. Gaukås, G. H. Olsen, J. Glaum, T. Tybell, and S. M. Selbach, "Interstitial oxygen as a source of  $p$ -type conductivity in hexagonal manganites," *Nat. Commun.* **7**, 13745 (2016).
- <sup>41</sup>J. Kasahara, T. Katayama, S. Mo, A. Chikamatsu, Y. Hamasaki, S. Yasui, M. Itoh, and T. Hasegawa, "Room-temperature antiferroelectricity in multiferroic hexagonal rare-earth ferrites," *ACS Appl. Mater. Interfaces* **13**, 4230–4235 (2021).
- <sup>42</sup>L. Wu, C. Y. Jimmy, L. Zhang, X. Wang, and S. Li, "Selective self-propagating combustion synthesis of hexagonal and orthorhombic nanocrystalline yttrium iron oxide," *J. Solid State Chem.* **177**, 3666–3674 (2004).
- <sup>43</sup>Y. Zhang, J. Yang, J. Xu, Q. Gao, and Z. Hong, "Controllable synthesis of hexagonal and orthorhombic  $\text{YFeO}_3$  and their visible-light photocatalytic activities," *Mater. Lett.* **81**, 1–4 (2012).
- <sup>44</sup>B. Zhang, M. Seki, H. Zhou, J. Chen, and H. Tabata, " $\text{InFeO}_3$  photoelectrode with two-dimensional superlattice for visible- and ultraviolet-light-driven water splitting," *APL Mater.* **8**, 051107 (2020).
- <sup>45</sup>D. Choudhury, A. Hazarika, A. Venimadhav, C. Kakarla, K. T. Delaney, P. S. Devi, P. Mondal, R. Nirmala, J. Gopalakrishnan, N. A. Spaldin, U. V. Waghmare, and D. D. Sarma, "Electric and magnetic polarizabilities of hexagonal  $\text{Ln}_2\text{CuTiO}_6$  ( $\text{Ln} = \text{Y}, \text{Dy}, \text{Ho}, \text{Er}, \text{and Yb}$ )," *Phys. Rev. B* **82**, 134203 (2010).
- <sup>46</sup>M. G. Kim, B. Winn, S. Chi, A. T. Savici, J. A. Rodriguez-Rivera, W. C. Chen, X. Xu, Y. Li, J. W. Kim, S.-W. Cheong, and V. Kiryukhin, "Spin-liquid-like state in pure and Mn-doped  $\text{TbInO}_3$  with a nearly triangular lattice," *Phys. Rev. B* **100**, 024405 (2019).
- <sup>47</sup>S. F. Weber, S. M. Griffin, and J. B. Neaton, "Topological semimetal features in the multiferroic hexagonal manganites," *Phys. Rev. Mater.* **3**, 064206 (2019).
- <sup>48</sup>C. Lu, L.-D. Zhang, X. Wu, F. Yang, and J. Hu, " $d+id$  chiral superconductivity in a triangular lattice from trigonal bipyramidal complexes," *Phys. Rev. B* **97**, 165110 (2018).
- <sup>49</sup>J. Nordlander, M. Campanini, M. D. Rossell, R. Erni, Q. N. Meier, A. Cano, N. Spaldin, M. Fiebig, and M. Trassin, "The ultrathin limit of improper ferroelectricity," *Nat. Commun.* **10**, 5591 (2019).
- <sup>50</sup>J. A. Mundy, C. M. Brooks, M. E. Holtz, J. A. Moyer, H. Das, A. F. Rébola, J. T. Heron, J. D. Clarkson, S. M. Disseler, Z. Liu, A. Farhan, R. Held, R. Hovden, E. Padgett, Q. Mao, H. Paik, R. Misra, L. F. Kourkoutis, E. Arenholz, A. Scholl, J. A. Borchers, W. D. Ratcliff, R. Ramesh, C. J. Fennie, P. Schiffer, D. A. Muller, and D. G. Schlom, "Atomically engineered ferroic layers yield a room-temperature magnetoelectric multiferroic," *Nature* **537**, 523–527 (2016).
- <sup>51</sup>L. M. Garten, Z. Jiang, H. Paik, J. D. Perkins, A. Kakekhani, R. Fei, D. J. Werder, M. E. Holtz, D. S. Ginley, A. M. Rappe, D. E. Schlom, and M. L. Staruch, "Stromataxic stabilization of a metastable layered  $\text{ScFeO}_3$  polymorph," *Chem. Mater.* **33**, 7423–7431 (2021).
- <sup>52</sup>R. D. Shannon and C. T. Prewitt, "Revised values of effective ionic radii," *Acta Crystallogr., Sect. B: Struct. Crystallogr. Cryst. Chem.* **26**, 1046–1048 (1970).
- <sup>53</sup>R. I. Hines, "Atomistic simulation and *ab initio* studies of polar solids," Ph.D. thesis (University of Bristol, 1997).
- <sup>54</sup>D. Reinen, "The Jahn–Teller effect in solid state chemistry of transition metal compounds," *J. Solid State Chem.* **27**, 71–85 (1979).
- <sup>55</sup>K. Kamata, T. Nakajima, and T. Nakamura, "Thermogravimetric study of rare earth manganites  $\text{AMnO}_3$  ( $\text{A} = \text{Sm}, \text{Dy}, \text{Y}, \text{Er}, \text{Yb}$ ) at 1200 C," *Mater. Res. Bull.* **14**, 1007–1012 (1979).
- <sup>56</sup>K.-H. Hellwege, *Landolt Bornstein, Numerical Data And Functional Relationship In Science And Technology, Elastic, Piezoelectric, Pyroelectric, Piezooptic, Electrooptic Constants, and Nonlinear Dielectric Susceptibilities of Crystal* (Springer, 1979).
- <sup>57</sup>K. Nagashio and K. Kuribayashi, "Metastable phase formation from an under-cooled rare-earth orthoferrite melt," *J. Am. Ceram. Soc.* **85**, 2550–2556 (2002).
- <sup>58</sup>T. Katayama, Y. Hamasaki, S. Yasui, A. Miyahara, and M. Itoh, "Epitaxial thin film growth of garnet-,  $\text{GdFeO}_3$ -, and  $\text{YMnO}_3$ -type  $\text{LuFeO}_3$  using pulsed laser deposition," *Thin Solid Films* **642**, 41–44 (2017).
- <sup>59</sup>R. Uecker, R. Bertram, M. Brützmam, Z. Galazka, T. M. Gering, C. Guguschev, D. Klimm, M. Klupsch, A. Kwasniewski, and D. G. Schlom, "Large-lattice-parameter perovskite single-crystal substrates," *J. Cryst. Growth* **457**, 137–142 (2017).
- <sup>60</sup>N. Fujimura, T. Ishida, T. Yoshimura, and T. Ito, "Epitaxially grown  $\text{YMnO}_3$  film: New candidate for nonvolatile memory devices," *Appl. Phys. Lett.* **69**, 1011–1013 (1996).
- <sup>61</sup>V. Laukhin, V. Skumryev, X. Martí, D. Hrabovsky, F. Sánchez, M. V. García-Cuenca, C. Ferrater, M. Varela, U. Lüders, J. F. Bobo, and J. Fontcuberta, "Electric-field control of exchange bias in multiferroic epitaxial heterostructures," *Phys. Rev. Lett.* **97**, 227201 (2006).
- <sup>62</sup>D. Lee, A. Yoon, S. Y. Jang, J. G. Yoon, J. S. Chung, M. Kim, J. F. Scott, and T. W. Noh, "Giant flexoelectric effect in ferroelectric epitaxial thin films," *Phys. Rev. Lett.* **107**, 057602 (2011).
- <sup>63</sup>T. Jungk, Á. Hoffmann, M. Fiebig, and E. Soergel, "Electrostatic topology of ferroelectric domains in  $\text{YMnO}_3$ ," *Appl. Phys. Lett.* **97**, 12904 (2010).
- <sup>64</sup>N. Sai, C. J. Fennie, and A. A. Demkov, "Absence of critical thickness in an ultrathin improper ferroelectric film," *Phys. Rev. Lett.* **102**, 107601 (2009).
- <sup>65</sup>A. Bortis, M. Trassin, M. Fiebig, and T. Lottermoser, "Manipulation of charged domain walls in geometric improper ferroelectric thin films: A phase-field study," *Phys. Rev. Mater.* **6**, 064403 (2022).
- <sup>66</sup>J. Dho, C. W. Leung, J. L. MacManus-Driscoll, and M. G. Blamire, "Epitaxial and oriented  $\text{YMnO}_3$  film growth by pulsed laser deposition," *J. Cryst. Growth* **267**, 548–553 (2004).



- <sup>67</sup>A. Bosak, C. Dubourdieu, J.-P. Sénateur, O. Y. Gorbenko, and A. Kaul, "Epitaxial stabilization of hexagonal RMnO<sub>3</sub> (R = Eu-Dy) manganites," *J. Mater. Chem.* **12**, 800–801 (2002).
- <sup>68</sup>J.-W. Kim, L. Schultz, K. Dörr, B. B. Van Aken, and M. Fiebig, "Growth and multiferroic properties of hexagonal HoMnO<sub>3</sub> films," *Appl. Phys. Lett.* **90**, 012502 (2007).
- <sup>69</sup>I. Gélard, C. Dubourdieu, S. Pailhès, S. Petit, and C. Simon, "Neutron diffraction study of hexagonal manganite YMnO<sub>3</sub>, HoMnO<sub>3</sub>, and ErMnO<sub>3</sub> epitaxial films," *Appl. Phys. Lett.* **92**, 232506 (2008).
- <sup>70</sup>S. Y. Jang, D. Lee, J.-H. Lee, T. W. Noh, Y. Jo, M.-H. Jung, and J.-S. Chung, "Oxygen vacancy induced re-entrant spin glass behavior in multiferroic ErMnO<sub>3</sub> thin films," *Appl. Phys. Lett.* **93**, 162507 (2008).
- <sup>71</sup>A. Posadas, J.-B. Yau, and C. H. Ahn, "Epitaxial multiferroic hexagonal manganite thin films grown on ZnO," *Physica Status Solidi B* **243**, 2085–2088 (2006).
- <sup>72</sup>T. Takahashi, T. Yoshimura, and N. Fujimura, "Growth and ferromagnetic properties of ferroelectric YbMnO<sub>3</sub> thin films," *Jpn. J. Appl. Phys., Part I* **45**, 7329–7331 (2006).
- <sup>73</sup>K. R. Balasubramian, S. Havelia, P. A. Salvador, H. Zheng, and J. F. Mitchell, "Epitaxial stabilization and structural properties of REMnO<sub>3</sub> (RE = Dy, Gd, Sm) compounds in a layered, hexagonal ABO<sub>3</sub> structure," *Appl. Phys. Lett.* **91**, 232901 (2007).
- <sup>74</sup>J.-H. Lee, P. Murugavel, H. Ryu, D. Lee, J. Y. Jo, J. W. Kim, H. J. Kim, K. H. Kim, Y. Jo, M.-H. Jung, Y. H. Oh, Y.-W. Kim, J.-G. Yoon, J.-S. Chung, and T. W. Noh, "Epitaxial stabilization of a new multiferroic hexagonal phase of TbMnO<sub>3</sub> thin films," *Adv. Mater.* **18**, 3125–3129 (2006).
- <sup>75</sup>R. Mandal, M. Hirsbrunner, V. Roddatis, R. Gruhl, L. Schüller, U. Roß, S. Merten, P. Gegenwart, and V. Moshnyaga, "Strain-driven structure-ferroelectricity relationship in hexagonal TbMnO<sub>3</sub> films," *Phys. Rev. B* **102**, 104106 (2020).
- <sup>76</sup>C. R. Serrao, S. B. Krupanidhi, J. Bhattacharjee, U. V. Waghmare, A. K. Kundu, and C. N. R. Rao, "InMnO<sub>3</sub>: A biferroic," *J. Appl. Phys.* **100**, 076104 (2006).
- <sup>77</sup>Y. Kumagai, A. A. Belik, M. Lilienblum, N. Leo, M. Fiebig, and N. A. Spaldin, "Observation of persistent centrosymmetry in the hexagonal manganite family," *Phys. Rev. B* **85**, 174422 (2012).
- <sup>78</sup>F. T. Huang, X. Wang, S. M. Griffin, Y. Kumagai, O. Gindele, M. W. Chu, Y. Horibe, N. A. Spaldin, and S. W. Cheong, "Duality of topological defects in hexagonal manganites," *Phys. Rev. Lett.* **113**, 267602 (2014).
- <sup>79</sup>S. M. Griffin, M. Reidulff, S. M. Selbach, and N. A. Spaldin, "Defect chemistry as a crystal structure design parameter: Intrinsic point defects and Ga substitution in InMnO<sub>3</sub>," *Chem. Mater.* **29**, 2425–2434 (2017).
- <sup>80</sup>N. Jehanathan, O. Lebedev, I. Gélard, C. Dubourdieu, and G. Van Tendeloo, "Structure and defect characterization of multiferroic ReMnO<sub>3</sub> films and multilayers by TEM," *Nanotechnology* **21**, 075705 (2010).
- <sup>81</sup>J. Nordlander, M. D. Rossell, M. Campanini, M. Fiebig, and M. Trassin, "Epitaxial integration of improper ferroelectric hexagonal YMnO<sub>3</sub> thin films in heterostructures," *Phys. Rev. Mater.* **4**, 124403 (2020).
- <sup>82</sup>T. Choi and J. Lee, "Bi modification for low-temperature processing of YMnO<sub>3</sub> thin films," *Appl. Phys. Lett.* **84**, 5043–5045 (2004).
- <sup>83</sup>S. Imada, S. Shouriki, E. Tokumitsu, and H. Ishiura, "Epitaxial growth of ferroelectric YMnO<sub>3</sub> thin films on Si (111) substrates by molecular beam epitaxy," *Jpn. J. Appl. Phys.* **37**, 6497–6501 (1998).
- <sup>84</sup>S. Imada, T. Kuraoka, E. Tokumitsu, and H. Ishiura, "Ferroelectricity of YMnO<sub>3</sub> thin films on Pt(111)/Al<sub>2</sub>O<sub>3</sub>(0001) and Pt(111)/Y<sub>2</sub>O<sub>3</sub>(111)/Si(111) structures grown by molecular beam epitaxy," *Jpn. J. Appl. Phys., Part I* **40**, 666–671 (2001).
- <sup>85</sup>X. Martí, F. Sánchez, D. Hrabovsky, J. Fontcuberta, V. Laukhin, V. Skumryev, M. V. García-Cuenca, C. Ferrater, M. Varela, U. Lüders, J. F. Bobo, S. Estradé, J. Arbiol, and F. Peiró, "Epitaxial growth of biferroic YMnO<sub>3</sub>(0 0 0 1) on platinum electrodes," *J. Cryst. Growth* **299**, 288–294 (2007).
- <sup>86</sup>K. H. Wu, H.-J. Chen, Y. T. Chen, C. C. Hsieh, C. W. Luo, T. M. Uen, J. Y. Juang, J.-Y. Lin, T. Kobayashi, and M. Gospodinov, "Marked enhancement of Néel temperature in strained YMnO<sub>3</sub> thin films probed by femtosecond spectroscopy," *Europhys. Lett.* **94**, 27006 (2011).
- <sup>87</sup>Y. Chye, T. Liu, D. Li, K. Lee, D. Lederman, and T. H. Myers, "Molecular beam epitaxy of YMnO<sub>3</sub> on c-plane GaN," *Appl. Phys. Lett.* **88**, 132903 (2006).
- <sup>88</sup>S. Cheng, C. Xu, S. Deng, M.-G. Han, S. Bao, J. Ma, C. Nan, W. Duan, L. Bellaiche, Y. Zhu, and J. Zhu, "Interface reconstruction with emerging charge ordering in hexagonal manganite," *Sci. Adv.* **4**, eaar4298 (2018).
- <sup>89</sup>H. Pang, F. Zhang, M. Zeng, X. Gao, M. Qin, X. Lu, J. Gao, J. Dai, and Q. Li, "Preparation of epitaxial hexagonal YMnO<sub>3</sub> thin films and observation of ferroelectric vortex domains," *npj Quantum Mater.* **1**, 16015 (2016).
- <sup>90</sup>D. J. Kim, J. G. Connell, S. S. A. Seo, and A. Gruverman, "Domain wall conductivity in semiconducting hexagonal ferroelectric TbMnO<sub>3</sub> thin films," *Nanotechnology* **27**, 155705 (2016).
- <sup>91</sup>J. Fontcuberta, "Multiferroic RMnO<sub>3</sub> thin films," *C. R. Phys.* **16**, 204–226 (2015).
- <sup>92</sup>S. Cheng, M. Li, S. Deng, S. Bao, P. Tang, W. Duan, J. Ma, C. Nan, and J. Zhu, "Manipulation of magnetic properties by oxygen vacancies in multiferroic YMnO<sub>3</sub>," *Adv. Funct. Mater.* **26**, 3589–3598 (2016).
- <sup>93</sup>T. Kordel, C. Wehrenfennig, D. Meier, T. Lottermoser, M. Fiebig, I. Gélard, C. Dubourdieu, J. W. Kim, L. Schultz, and K. Dörr, "Nanodomains in multiferroic hexagonal RMnO<sub>3</sub> films (R = Y, Dy, Ho, Er)," *Phys. Rev. B* **80**, 045409 (2009).
- <sup>94</sup>M. Giraldo, Q. N. Meier, A. Bortis, D. Nowak, N. A. Spaldin, M. Fiebig, M. C. Weber, and T. Lottermoser, "Magnetoelectric coupling of domains, domain walls and vortices in a multiferroic with independent magnetic and electric order," *Nat. Commun.* **12**, 3093 (2021).
- <sup>95</sup>Y. Zhang, W. Si, Y. Jia, P. Yu, R. Yu, and J. Zhu, "Controlling strain relaxation by interface design in highly lattice-mismatched heterostructure," *Nano Lett.* **21**, 6867–6874 (2021).
- <sup>96</sup>S. Artyukhin, K. T. Delaney, N. A. Spaldin, and M. Mostovoy, "Landau theory of topological defects in multiferroic hexagonal manganites," *Nat. Mater.* **13**, 42–49 (2014).
- <sup>97</sup>X. Wang, M. Mostovoy, M. G. Han, Y. Horibe, T. Aoki, Y. Zhu, and S.-W. Cheong, "Unfolding of vortices into topological stripes in a multiferroic material," *Phys. Rev. Lett.* **112**, 247601 (2014).
- <sup>98</sup>H. Tan, C. Xu, M. Li, S. Wang, B.-L. Gu, and W. Duan, "Pressure and strain effects of hexagonal rare-earth manganites: A first-principles study," *J. Phys.: Condens. Matter* **28**, 126002 (2016).
- <sup>99</sup>C. Dubourdieu, G. Huot, I. Gélard, H. Roussel, O. Lebedev, and G. Van Tendeloo, "Thin films and superlattices of multiferroic hexagonal rare earth manganites," *Philos. Mag. Lett.* **87**, 203–210 (2007).
- <sup>100</sup>J. Nordlander, M. D. Rossell, M. Campanini, M. Fiebig, and M. Trassin, "Inversion-symmetry engineering in layered oxide thin films," *Nano Lett.* **21**, 2780–2785 (2021).
- <sup>101</sup>J. Nordlander, N. Strkalj, M. Fiebig, and M. Trassin, "Probing ferroic states in oxide thin films using optical second harmonic generation," *Appl. Sci.* **8**, 570 (2018).
- <sup>102</sup>M. F. Sarott, E. Gradauskaitė, J. Nordlander, N. Strkalj, and M. Trassin, "In situ monitoring of epitaxial ferroelectric thin-film growth," *J. Phys.: Condens. Matter* **33**, 293001 (2021).
- <sup>103</sup>N. Kumar, S. Najmaei, Q. Cui, F. Ceballos, P. M. Ajayan, J. Lou, and H. Zhao, "Second harmonic microscopy of monolayer MoS<sub>2</sub>," *Phys. Rev. B* **87**, 161403 (2013).
- <sup>104</sup>S. Geller, J. B. Jeffries, and P. J. Curlander, "The crystal structure of a new high-temperature modification of YGaO<sub>3</sub>," *Acta Crystallogr., Sect. B Struct. Crystallogr. Cryst. Chem.* **31**, 2770–2774 (1975).
- <sup>105</sup>C. Pistorius and G. Kruger, "Stability and structure of noncentrosymmetric hexagonal LnInO<sub>3</sub> (Ln = Eu, Gd, Tb, Dy, Ho, Y)," *J. Inorg. Nucl. Chem.* **38**, 1471–1475 (1976).
- <sup>106</sup>R. Shukla, V. Grover, K. Srinivasu, B. Paul, A. Roy, R. Gupta, and A. K. Tyagi, "Rare earth indates (RE: La-Yb): Influence of the synthesis route and heat treatment on the crystal structure," *Dalton Trans.* **47**, 6787–6799 (2018).
- <sup>107</sup>I. Nodari, A. Alebouyeh, J. Brice, R. Gérardin, and O. Evrard, "Caracterisation de nouveaux ferrites d'indium: In<sub>2</sub>Fe<sub>4</sub>O<sub>9</sub> et InFeO<sub>3</sub>," *Mater. Res. Bull.* **23**, 1039–1044 (1988).
- <sup>108</sup>D. M. Giaquinta, W. M. Davis, and H. C. zur Loye, "Structure of indium iron oxide," *Acta Crystallogr., Sect. C: Cryst. Struct. Commun.* **50**, 5–7 (1994).
- <sup>109</sup>M. Seki, T. Konya, K. Inaba, and H. Tabata, "Epitaxial thin films of InFe<sub>2</sub>O<sub>4</sub> and InFeO<sub>3</sub> with two-dimensional triangular lattice structures grown by pulsed laser deposition," *Appl. Phys. Express* **3**, 105801 (2010).

- <sup>110</sup>M. E. Holtz, E. S. Padgett, R. Steinhardt, C. M. Brooks, D. Meier, D. G. Schlom, D. A. Muller, and J. A. Mundy, "Dimensionality-induced change in topological order in multiferroic oxide superlattices," *Phys. Rev. Lett.* **126**, 157601 (2021).
- <sup>111</sup>P. Vogt and O. Bierwagen, "The competing oxide and sub-oxide formation in metal-oxide molecular beam epitaxy," *Appl. Phys. Lett.* **106**, 081910 (2015).
- <sup>112</sup>O. Y. Gorbenko, S. Samoilenov, I. Graboy, and A. Kaul, "Epitaxial stabilization of oxides in thin films," *Chem. Mater.* **14**, 4026–4043 (2002).
- <sup>113</sup>P. Dankov, "Laws of the formation and structure of protective films on metals," *Proc. (Dokl.) Acad. Sci. USSR* **23**, 548 (1939).
- <sup>114</sup>Y. Hamasaki, T. Shimizu, S. Yasui, T. Taniyama, O. Sakata, and M. Itoh, "Crystal isomers of  $\text{ScFeO}_3$ ," *Cryst. Growth Des.* **16**, 5214–5222 (2016).
- <sup>115</sup>A. Bosak, A. Kamenev, I. Graboy, S. Antonov, O. Y. Gorbenko, A. Kaul, C. Dubourdieu, J. Senateur, V. Svechnikov, H. Zandbergen, and B. Holländer, "Epitaxial phase stabilisation phenomena in rare earth manganites," *Thin Solid Films* **400**, 149–153 (2001).
- <sup>116</sup>F. Moussa, M. Hennion, J. Rodriguez-Carvajal, H. Moudén, L. Pinsard, and A. Revcolevschi, "Spin waves in the antiferromagnet perovskite  $\text{LaMnO}_3$ : A neutron-scattering study," *Phys. Rev. B* **54**, 15149 (1996).
- <sup>117</sup>S. Geller and E. Wood, "Crystallographic studies of perovskite-like compounds. I. Rare earth orthoferrites and  $\text{YFeO}_3$ ,  $\text{YCrO}_3$ ,  $\text{YAlO}_3$ ," *Acta Crystallogr.* **9**, 563–568 (1956).
- <sup>118</sup>*Ternary Compounds, Organic Semiconductors*, Landolt-Börnstein—Group III Condensed Matter Vol. 41E, edited by O. Madelung, U. Rössler, and M. Schulz (Springer-Verlag, Berlin/Heidelberg, 2000).
- <sup>119</sup>M. Robbins, G. Wertheim, A. Menth, and R. Sherwood, "Preparation and properties of polycrystalline cerium orthoferrite ( $\text{CeFeO}_3$ )," *J. Phys. Chem. Solids* **30**, 1823–1825 (1969).
- <sup>120</sup>B. Dabrowski, S. Kolesnik, A. Baszczuk, O. Chmaissem, T. Maxwell, and J. Mais, "Structural, transport, and magnetic properties of  $\text{RMnO}_3$  perovskites ( $R = \text{La, Pr, Nd, Sm, }^{153}\text{Eu, Dy}$ )," *J. Solid State Chem.* **178**, 629–637 (2005).
- <sup>121</sup>G. J. McCarthy, P. V. Gallagher, and C. Sipe, "Crystal chemistry of catalytic materials. I. Composition and unit cell parameters of 'REMnO<sub>3</sub>' phases prepared in air," *Mater. Res. Bull.* **8**, 1277–1284 (1973).
- <sup>122</sup>A. A. Bossak, I. E. Graboy, O. Y. Gorbenko, A. R. Kaul, M. S. Kartavtseva, V. L. Svetchnikov, and H. W. Zandbergen, "XRD and HREM studies of epitaxially stabilized hexagonal orthoferrites  $\text{RFeO}_3$  ( $R = \text{Eu-Lu}$ )," *Chem. Mater.* **16**, 1751–1755 (2004).
- <sup>123</sup>S. Quezel, F. Tcheou, J. Rossat-Mignod, G. Quezel, and E. Roudaut, "Magnetic structure of the perovskite-like compound  $\text{TbMnO}_3$ ," *Physica B+C* **86**, 916–918 (1977).
- <sup>124</sup>M. Marezio, J. Remeika, and P. Dernier, "The crystal chemistry of the rare earth orthoferrites," *Acta Crystallogr., Sect. B: Struct. Crystallogr. Cryst. Chem.* **26**, 2008–2022 (1970).
- <sup>125</sup>W. C. Chueh, F. E. Gabaly, J. D. Sugar, N. C. Bartelt, A. H. McDaniel, K. R. Fenton, K. R. Zavadil, T. Tyliczszak, W. Lai, and K. F. McCarty, "Intercalation pathway in many-particle  $\text{LiFePO}_4$  electrode revealed by nanoscale state-of-charge mapping," *Nano Lett.* **13**, 866–872 (2013).
- <sup>126</sup>A. Akbashev, V. Roddatis, A. Vasiliev, S. Lopatin, V. Amelichev, and A. Kaul, "Reconstruction of the polar interface between hexagonal  $\text{LuFeO}_3$  and intergrown  $\text{Fe}_3\text{O}_4$  nanolayers," *Sci. Rep.* **2**, 672 (2012).
- <sup>127</sup>J. Greedan, M. Bieringer, J. Britten, D. Giaquinta, and H.-C. Zur Loye, "Synthesis, crystal structure, and unusual magnetic properties of  $\text{InMnO}_3$ ," *J. Solid State Chem.* **116**, 118–130 (1995).
- <sup>128</sup>Y. Bréard, H. Fjellvåg, and B. Hauback, "Investigation of bixbyite type scandium oxides involving a magnetic cation:  $\text{Sc}_{2-x}\text{Fe}_x\text{O}_3$  ( $0 \leq x \leq 1$ )," *Solid State Commun.* **151**, 223–226 (2011).
- <sup>129</sup>M. F. Bekheet, I. Svoboda, N. Liu, L. Bayarjargal, E. Irran, C. Dietz, R. W. Stark, R. Riedel, and A. Guro, "Ferroelectric  $\text{InMnO}_3$ : Growth of single crystals, structure and high-temperature phase transitions," *J. Solid State Chem.* **241**, 54–63 (2016).
- <sup>130</sup>S.-J. Ahn, J.-H. Lee, Y. K. Jeong, E.-H. Na, Y. M. Koo, and H. M. Jang, "Artificially imposed hexagonal ferroelectricity in canted antiferromagnetic  $\text{YFeO}_3$  epitaxial thin films," *Mater. Chem. Phys.* **138**, 929–936 (2013).
- <sup>131</sup>X. Xu and W. Wang, "Multiferroic hexagonal ferrites ( $\text{h-RFeO}_3$ ,  $R = \text{Y, Dy-Lu}$ ): A brief experimental review," *Mod. Phys. Lett. B* **28**, 1430008 (2014).
- <sup>132</sup>J. A. Moyer, R. Misra, J. A. Mundy, C. M. Brooks, J. T. Heron, D. A. Muller, D. G. Schlom, and P. Schiffer, "Intrinsic magnetic properties of hexagonal  $\text{LuFeO}_3$  and the effects of nonstoichiometry," *APL Mater.* **2**, 012106 (2014).
- <sup>133</sup>Y. K. Jeong, J.-H. Lee, S.-J. Ahn, and H. M. Jang, "Epitaxially constrained hexagonal ferroelectricity and canted triangular spin order in  $\text{LuFeO}_3$  thin films," *Chem. Mater.* **24**, 2426–2428 (2012).
- <sup>134</sup>P. Barrozo, D. R. Småbråten, Y. Tang, B. Prasad, S. Saremi, R. Ozgur, V. Thakare, R. A. Steinhardt, M. E. Holtz, V. A. Stoica, L. W. Martin, D. G. Schlom, S. M. Selbach, and R. Ramesh, "Defect-enhanced polarization switching in the improper ferroelectric  $\text{LuFeO}_3$ ," *Adv. Mater.* **32**, 2000508 (2020).
- <sup>135</sup>J. Casamento, M. E. Holtz, H. Paik, P. Dang, R. Steinhardt, H. Xing, D. G. Schlom, and D. Jena, "Multiferroic  $\text{LuFeO}_3$  on GaN by molecular-beam epitaxy," *Appl. Phys. Lett.* **116**, 102901 (2020).
- <sup>136</sup>A. R. Akbashev, V. V. Roddatis, A. L. Vasiliev, S. Lopatin, A. S. Semisalova, N. S. Perov, V. A. Amelichev, and A. R. Kaul, "Reconstructed stacking faults in cobalt-doped hexagonal  $\text{LuFeO}_3$  revealed by mapping of cation distribution at the atomic scale," *CrystEngComm* **14**, 5373–5376 (2012).
- <sup>137</sup>D. Lee, J.-H. Lee, P. Murugavel, S. Jang, T. Noh, Y. Jo, M.-H. Jung, Y.-D. Ko, and J.-S. Chung, "Epitaxial stabilization of artificial hexagonal  $\text{GdMnO}_3$  thin films and their magnetic properties," *Appl. Phys. Lett.* **90**, 182504 (2007).
- <sup>138</sup>S. Harikrishnan, S. Rößler, C. N. Kumar, H. Bhat, U. Rößler, S. Wirth, F. Steglich, and S. Elizabeth, "Phase transitions and rare-earth magnetism in hexagonal and orthorhombic  $\text{DyMnO}_3$  single crystals," *J. Phys.: Condens. Matter* **21**, 096002 (2009).
- <sup>139</sup>J. Iida, S. Takekawa, and N. Kimizuka, "Single crystal growth of  $\text{LuFe}_2\text{O}_4$ ,  $\text{LuFeCoO}_4$  and  $\text{YbFeMgO}_4$  by the floating zone method," *J. Cryst. Growth* **102**, 398–400 (1990).
- <sup>140</sup>R. A. Steinhardt, C. M. Brooks, G. C. Correa, M. E. Holtz, R. Ramesh, D. A. Muller, J. A. Mundy, and D. G. Schlom, " $\text{DyFe}_2\text{O}_4$ : A new trigonal rare-earth ferrite grown by molecular-beam epitaxy," *APL Mater.* **9**, 041106 (2021).
- <sup>141</sup>H. Iida, T. Koizumi, Y. Uesu, K. Kohn, N. Ikeda, S. Mori, R. Haumont, P.-E. Janolin, J.-M. Kiat, M. Fukunaga, and Y. Noda, "Ferroelectricity and ferrimagnetism of hexagonal  $\text{YbFeO}_3$  thin films," *J. Phys. Soc. Jpn.* **81**, 024719 (2012).
- <sup>142</sup>H. Yokota, T. Nozue, S. Nakamura, M. Fukunaga, and A. Fuwa, "Examination of ferroelectric and magnetic properties of hexagonal  $\text{ErFeO}_3$  thin films," *Jpn. J. Appl. Phys., Part I* **54**, 10NA10 (2015).
- <sup>143</sup>Y. Hamasaki, T. Katayama, S. Yasui, T. Shiraishi, A. Akama, T. Kiguchi, T. Taniyama, and M. Itoh, "Switchable third  $\text{ScFeO}_3$  polar ferromagnet with  $\text{YMnO}_3$ -type structure," *J. Mater. Chem. C* **8**, 4447–4452 (2020).
- <sup>144</sup>J. Li, U. G. Singh, T. D. Schladt, J. K. Stalick, S. L. Scott, and R. Seshadri, "Hexagonal  $\text{YFe}_{1-x}\text{Pd}_x\text{O}_{3-\delta}$ : Nonperovskite host compounds for  $\text{Pd}^{2+}$  and their catalytic activity for CO oxidation," *Chem. Mater.* **20**, 6567–6576 (2008).
- <sup>145</sup>A. A. Belik, S. Kamba, M. Savinov, D. Nuzhnyy, M. Tachibana, E. Takayama-Muromachi, and V. Goian, "Magnetic and dielectric properties of hexagonal  $\text{InMnO}_3$ ," *Phys. Rev. B* **79**, 054411 (2009).
- <sup>146</sup>B. Paul, S. Chatterjee, S. Gop, A. Roy, V. Grover, R. Shukla, and A. Tyagi, "Evolution of lattice dynamics in ferroelectric hexagonal  $\text{REInO}_3$  ( $\text{RE} = \text{Ho, Dy, Tb, Gd, Eu, Sm}$ ) perovskites," *Mater. Res. Express* **3**, 075703 (2016).
- <sup>147</sup>U. Adem, A. A. Nugroho, A. Meetsma, and T. Palstra, "Ferroelectric displacements in multiferroic  $\text{Y}(\text{Mn,Ga})\text{O}_3$ ," *Phys. Rev. B* **75**, 014108 (2007).